

## Microkinetic Modeling: A Tool for Rational Catalyst Design

Ali Hussain Motagamwala\* and James A. Dumesic\*

Cite This: *Chem. Rev.* 2021, 121, 1049–1076

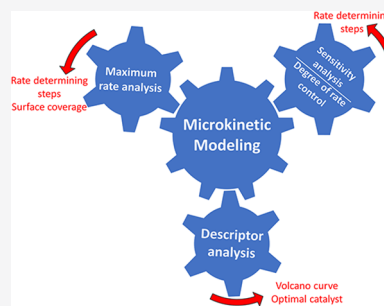
Read Online

ACCESS |

Metrics &amp; More

Article Recommendations

**ABSTRACT:** The design of heterogeneous catalysts relies on understanding the fundamental surface kinetics that controls catalyst performance, and microkinetic modeling is a tool that can help the researcher in streamlining the process of catalyst design. Microkinetic modeling is used to identify critical reaction intermediates and rate-determining elementary reactions, thereby providing vital information for designing an improved catalyst. In this review, we summarize general procedures for developing microkinetic models using reaction kinetics parameters obtained from experimental data, theoretical correlations, and quantum chemical calculations. We examine the methods required to ensure the thermodynamic consistency of the microkinetic model. We describe procedures required for parameter adjustments to account for the heterogeneity of the catalyst and the inherent errors in parameter estimation. We discuss the analysis of microkinetic models to determine the rate-determining reactions using the degree of rate control and reversibility of each elementary reaction. We introduce incorporation of Brønsted–Evans–Polanyi relations and scaling relations in microkinetic models and the effects of these relations on catalytic performance and formation of volcano curves are discussed. We review the analysis of reaction schemes in terms of the maximum rate of elementary reactions, and we outline a procedure to identify kinetically significant transition states and adsorbed intermediates. We explore the application of generalized rate expressions for the prediction of optimal binding energies of important surface intermediates and to estimate the extent of potential rate improvement. We also explore the application of microkinetic modeling in homogeneous catalysis, electro-catalysis, and transient reaction kinetics. We conclude by highlighting the challenges and opportunities in the application of microkinetic modeling for catalyst design.



### CONTENTS

1. Introduction	1049
2. Formulation of a Microkinetic Model	1051
2.1. Formulation of a Reaction Mechanism	1052
2.2. Stoichiometric Consistency	1053
2.3. Equilibrium Constant Estimation	1054
2.4. Thermodynamic Consistency	1054
2.5. Rate Constant Estimation	1054
2.5.1. Collision Theory	1054
2.5.2. Transition State Theory	1055
2.6. Model Development	1055
2.7. Numerical Solution Strategies	1056
2.8. Parameters Adjustments and Self-Consistency in Microkinetic Modeling	1056
3. Analysis after Model Development	1057
3.1. Reversibility of Elementary Steps and Its Properties	1057
3.2. Sensitivity Analysis	1057
3.3. Degree of Rate Control	1057
3.4. Selectivity and Degree of Selectivity Control	1059
4. Brønsted–Evans–Polanyi and Scaling Correlations	1059
4.1. Scaled Degree of Rate Control	1061
5. Machine Learning in Microkinetic Modeling	1061
6. Maximum Rate Analysis	1062

7. Rate Expression Analysis	1064
8. Microkinetic Models in Homogeneous Catalysis	1065
9. Microkinetic Models in Electrocatalytic Application	1066
10. Microkinetic Modeling of Transient Kinetics	1066
Concluding Remarks and Outlook	1067
Appendix I	1068
Author Information	1068
Corresponding Authors	1068
Notes	1068
Biographies	1068
Acknowledgments	1069
Dedication	1069
References	1069

### 1. INTRODUCTION

Twenty years ago, Michel Boudart wrote:<sup>1</sup>

**Special Issue:** Advanced Materials and Methods for Catalysis and Electrocatalysis by Transition Metals

**Received:** May 1, 2020

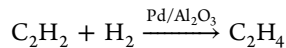
**Published:** November 18, 2020



"In the past, rate constants were extracted from rate equations obtained by fitting kinetic data. In the future, they will be calculated by computational chemistry or measured by surface science techniques. They will be used for the start-up of a microkinetic analysis in a combinatorial iteration for the development of optimized catalysts."

Twenty years later, the microkinetic analysis of the reaction mechanism is being used extensively in the identification of critical properties for catalyst design.

Catalysis is primarily a kinetic phenomenon and chemical kinetics is a vital tool in catalysis research. Reaction kinetics data are used in reactor design, in studying reaction mechanism, and in elucidating the structure–property relationship of a catalyst. As a first approximation, the kinetics of a chemical reaction can be expressed as a power–law expression by regressing experimental data. These reaction kinetics expressions are extensively used in controlling industrial reactors and predicting their performance over time owing to their simplicity and ease of application. For example, the selective hydrogenation of ethyne over a supported palladium catalyst is an industrially relevant reaction for polishing ethylene stream before polymerization:



The following power–law rate expression was obtained for hydrogenation of ethyne:

$$r = k[\text{P}_{\text{C}_2\text{H}_2}]^{\alpha_1}[\text{P}_{\text{H}_2}]^{\alpha_2} \quad (1)$$

where  $k$  is the rate constant that captures the temperature dependence of the reaction rate. The dependence of the rate on the activities of reactants and products is described in terms of reaction orders,  $\alpha_1$  and  $\alpha_2$ . After regression of experimental data, the value of  $\alpha_1$  is obtained between 0 and  $-0.7$  and  $\alpha_2$  is obtained between 1 and 1.5 depending on reaction conditions.<sup>2–4</sup> In most cases, the power–law rate expression is a limiting approximation of a more complex rate expression, and thus, the apparent activation energy and the reaction orders obtained by regression of experimental data are valid for a limited range of reaction conditions. Additionally, limited fundamental insight regarding the reaction mechanism can be obtained from simple power–law expressions. However, due to their simplicity and ease of use, the power–law expressions are appropriate for incorporating the effects of heat and mass transfer<sup>5</sup> as well as in some cases catalyst deactivation<sup>6</sup> in reactor design equations. As such, power–law rate expressions are widely used to operate industrial reactors.<sup>7,8</sup>

Depending upon the reaction conditions, the catalyst surface may become saturated with surface species and under certain reaction conditions, the reaction order with respect to certain reactant and products may become zero or negative. For example, in the power–law expression for ethyne hydrogenation (eq 1), the reaction order with respect to ethyne is negative, which indicates saturation of available active sites on the catalyst surface by ethyne adsorption. The inhibition of active sites can be accounted by a site blocking term in the rate expression. The Langmuir–Hinshelwood–Hougen–Watson (LHHW) rate expression includes such a site blocking term, and the general form of LHHW rate expression is:

$$\text{Rate} = \frac{(\text{kinetic term})(\text{thermodynamic driving term})}{(\text{adsorption or site blocking term})^n} \quad (2)$$

The kinetic term contains the forward rate constants of the rate-determining reactions, the equilibrium constants of the

equilibrated steps and the activity of the reactants forming the transition state of the rate-determining reactions. The thermodynamic driving term represents the closeness of the overall reaction to thermodynamic equilibrium.

The thermodynamic driving term is between 0 and 1, where 0 represents that the overall reaction is at equilibrium and 1 represents that overall reaction is far from equilibrium. The site blocking term is the inverse of the fraction of surface sites available for reaction, and the exponent,  $n$ , on the site blocking term is the number of surface sites participating in the rate determining reaction. The LHHW rate expression for a reaction mechanism is obtained by assuming certain rate determining elementary reactions, quasi-equilibrated elementary reactions, and the presence of most abundant surface intermediates (MASIs). For example, consider the reaction mechanism for ethyne hydrogenation shown in Table 1, assuming that the

**Table 1. Reaction Mechanism for Ethyne Hydrogenation**

#	elementary step <sup>a</sup>
1	$\text{H}_2 + 2^* \rightleftharpoons 2\text{H}^*$
2	$\text{C}_2\text{H}_2 + * \rightleftharpoons \text{C}_2\text{H}_2^*$
3	$\text{C}_2\text{H}_2^* + \text{H}^* \rightleftharpoons \text{C}_2\text{H}_3^* + *$
4	$\text{C}_2\text{H}_3^* + \text{H}^* \rightleftharpoons \text{C}_2\text{H}_4^* + *$
5	$\text{C}_2\text{H}_4^* \rightleftharpoons \text{C}_2\text{H}_4 + *$

<sup>a</sup>\* represents active site and X\* represents adsorbed species.

addition of the second hydrogen atom to the vinyl intermediates (step 4) as rate-determining step, all other elementary reactions as quasi-equilibrated steps and adsorbed hydrogen and ethyne as abundant surface intermediates. The following LHHW rate expression is obtained:

$$r = \frac{k_4 K_1 K_2 K_3 P_{\text{C}_2\text{H}_2} P_{\text{H}_2} (1 - \beta)}{(1 + K_2 P_{\text{C}_2\text{H}_2} + \sqrt{K_1 P_{\text{H}_2}})^2} \quad (3)$$

where  $k_4$  is the forward rate constant of the rate determining step,  $K_i$  is the equilibrium constant of step  $i$ ,  $\beta$  is the approach to equilibrium (also called the overall reversibility of the reaction), and the exponent in the denominator shows that the rate determining reaction involves two surface sites.

The LHHW rate expression is valid for a wider range of reaction conditions as compared to the power–law rate expression; however, the assumptions of Langmuir adsorption are implicit. Specifically, the LHHW rate expression assumes that all active sites for adsorption and reaction are identical and that interactions between adsorbed species are negligible. LHHW rate expressions are extensively used to model the performance of industrial reactors.<sup>9–11</sup> Improved reaction kinetics models are obtained when interaction between the surface species, atomic processes, and surface nonidealities are incorporated. A noteworthy example is the Temkin–Pyzhev equation wherein the rate of adsorption and desorption of nitrogen molecule is strongly dependent on the fraction of the catalyst surface covered by adsorbed atomic nitrogen.<sup>12–14</sup>

The traditional method outlined above provides useful information and researchers have used the information from these models coupled with chemical intuition to design better catalysts. In this respect, obtaining information regarding the fundamental surface chemistry occurring on the catalyst surface is highly desirable as it accelerates and streamlines the process of rational catalyst design. Microkinetic modeling does not make

initial assumptions about the nature of rate determining elementary reactions or most abundant surface intermediates, and it incorporates the essential surface chemistry on the catalyst. Various methods have been developed over time to perform microkinetic analysis, resulting in a large and important body of literature.<sup>15–42</sup>

Figure 1 shows the number of publication and the number of citations for reports on microkinetic modeling in the past three

discuss prediction of optimal binding energies of important surface intermediates as well as extent of potential rate improvement by generalized rate expressions. Lastly, we explore the application of microkinetic modeling in homogeneous catalysis, electro-catalysis, and transient reaction kinetics.

## 2. FORMULATION OF A MICROKINETIC MODEL

An important goal of research and development in industrial catalysis is to identify reaction conditions that lead to improved throughput and to develop catalytic material with improved performance. The former goal is generally achieved by using a reactor level model which enables the prediction of the system performance under various operating conditions. The latter goal relies heavily on previous experience with similar chemistry as well as chemical intuition. However, systematic elucidation of the reaction mechanism, which includes surface chemistry, can provide essential insights for the rapid development of catalysts with improved performance. Microkinetic modeling provides the framework for the analysis of reaction mechanism and provides valuable information about rate limiting reactions and abundant surface species such that research effort can be efficiently focused on designing catalytic materials with improved performance.

A general strategy for formulating a microkinetic model is to first develop a feasible reaction scheme that encompasses all elementary surface events occurring during the catalytic transformation of reactants to products, that is, all reactants and products, and plausible reaction intermediates are included in the reaction mechanism. However, the desire to include all reaction intermediates on the catalyst surface must be balanced with the need to express the reaction intermediates that are accessible to experimental measurement or theoretical prediction. Next, the thermodynamic properties of all adsorbed species and kinetic parameters for all elementary surface reactions are calculated or estimated. Since the reaction rate is controlled by only a few key parameters, that is, the activation energies of the rate determining reactions and adsorption energies of most abundant surface intermediate, precise values of all kinetic parameters are not required. However, it is not usually possible to know which kinetic parameters are rate-controlling and as such microkinetic studies are carried out with best possible estimates of the kinetic parameters.<sup>15</sup> Recently, methods using maximum rates of elementary steps or generalized rate expressions have been proposed to identify critical kinetic parameters such that detailed quantum chemical calculations are required for only a small subset of kinetic parameters and approximate values suffice for all other noncritical kinetic parameters.<sup>43</sup> Finally, the model is defined by a set of material balance equations. The set of material balance equation is solved to determine the surface coverages of all adsorbed species and the forward and reverse rates of all elementary steps for a range of reaction conditions. Sensitivity analyses can be carried out using this microkinetic model to identify the transition states and adsorbed species that control the reaction kinetics. Next, we discuss the process of developing a microkinetic model. We note here that the rate of reaction throughout this review refers to the reaction rate at steady state, except for the section on microkinetic modeling of transient reaction kinetics (section 10).

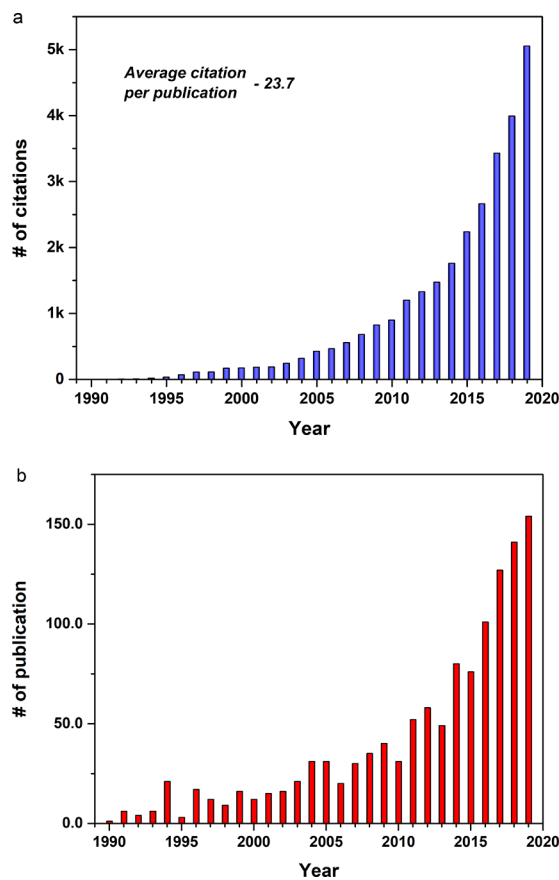


Figure 1. Microkinetic modeling in literature. (a) Number of citations and (b) number of publications. Results of a Web of Science search (as of March 31, 2020) for the term “Microkinetic modeling”.

decades. The rapid increase in studies utilizing microkinetic modeling is partially due to the improvements in computational techniques for determination of kinetic parameters and partially due to the success of microkinetic models in assisting rational catalyst design.

In this review, we first summarize a general procedure for developing microkinetic models using parameters obtained from quantum chemical calculations or other methods. We discuss various techniques including the degree of rate control for analysis of the microkinetic model. Then we discuss the incorporation of Brønsted–Evans–Polanyi correlations and scaling relations in microkinetic models and the effect of these correlation on catalytic performance and formation of volcano curves. We review some of the recent literature using microkinetic modeling for designing catalysts for industrially relevant reactions. We review the application of machine learning in microkinetic analysis. We also review the analysis of reaction schemes in term of the maximum rate of elementary reactions, and we outline a procedure to identify kinetically significant transition states and adsorbed intermediates. We

## 2.1. Formulation of a Reaction Mechanism

Catalytic processes proceed through combinations of elementary reactions. Table 2 shows some of the frequently encountered reaction types in heterogeneous catalysis.<sup>15</sup>

**Table 2. Surface Reaction Type and Examples (Adapted from Ref 15)**

#	reaction type	example <sup>a</sup>
1	molecular adsorption and desorption	$\text{N}_2 + * \rightleftharpoons \text{N}_2^*$
2	dissociative adsorption and desorption	$\text{N}_2 + 2* \rightleftharpoons 2\text{N}^*$
3	Langmuir–Hinshelwood reaction	$\text{N}^* + \text{H}^* \rightleftharpoons \text{NH}^*$
4	Eley–Rideal reaction	$\text{C}_2\text{H}_4 + \text{O}^* \rightleftharpoons \text{C}_2\text{H}_4\text{O}^*$
5	multisite intermediate formation	$\text{CO}^* + \text{OH}^* \rightleftharpoons \text{HCOO}^{**}$
6	multisite reaction <sup>b</sup>	$\text{N}^* + \text{H}^* \rightleftharpoons \text{NH}^* + #$

<sup>a</sup>\* represents a surface site. <sup>b</sup># represents another surface site distinct from \*

A sequence of elementary reactions based on the chemistry of the species involved is postulated as the mechanism of the overall reaction. In general, a reaction mechanism includes adsorption of reactants, surface transformation and desorption

of products. A reaction mechanism, however, can be complicated depending on the level of mechanistic detail that is included. For example, consider the reverse water gas-shift reaction over  $\text{MoO}_x$ -promoted  $\text{Au/SiO}_2$  catalyst, where it has been shown that interfacial sites (interface between Au and Mo) are an order of magnitude more active than under-coordinated Au sites.<sup>44</sup> A microkinetic model can be developed to include these distinct sites or a lumped model can be developed wherein a single site is designated to represent the reaction. In cases where distinct chemistry occurs on different active sites, for example catalytic cracking over mixed metal oxide or zeolites, it is instructive to include all distinct active sites in the mechanism and perform site balance on all distinct active sites (discussed in detail in section 2.6).<sup>27</sup> Thus, the level of mechanistic details included in the reaction mechanism depends on the goal of the model. Another complexity can be due to the sheer size of the reaction mechanism. For example, consider the expansive reaction mechanism for upgrading syngas shown in Figure 2a.<sup>45</sup> The complete reaction mechanism exhibits enormous complexity with hundreds of species and elementary reactions; however, this detailed mechanism is not necessary for most application as only a few intermediates and elementary reactions are significant. Therefore, it is the choice of the researcher to

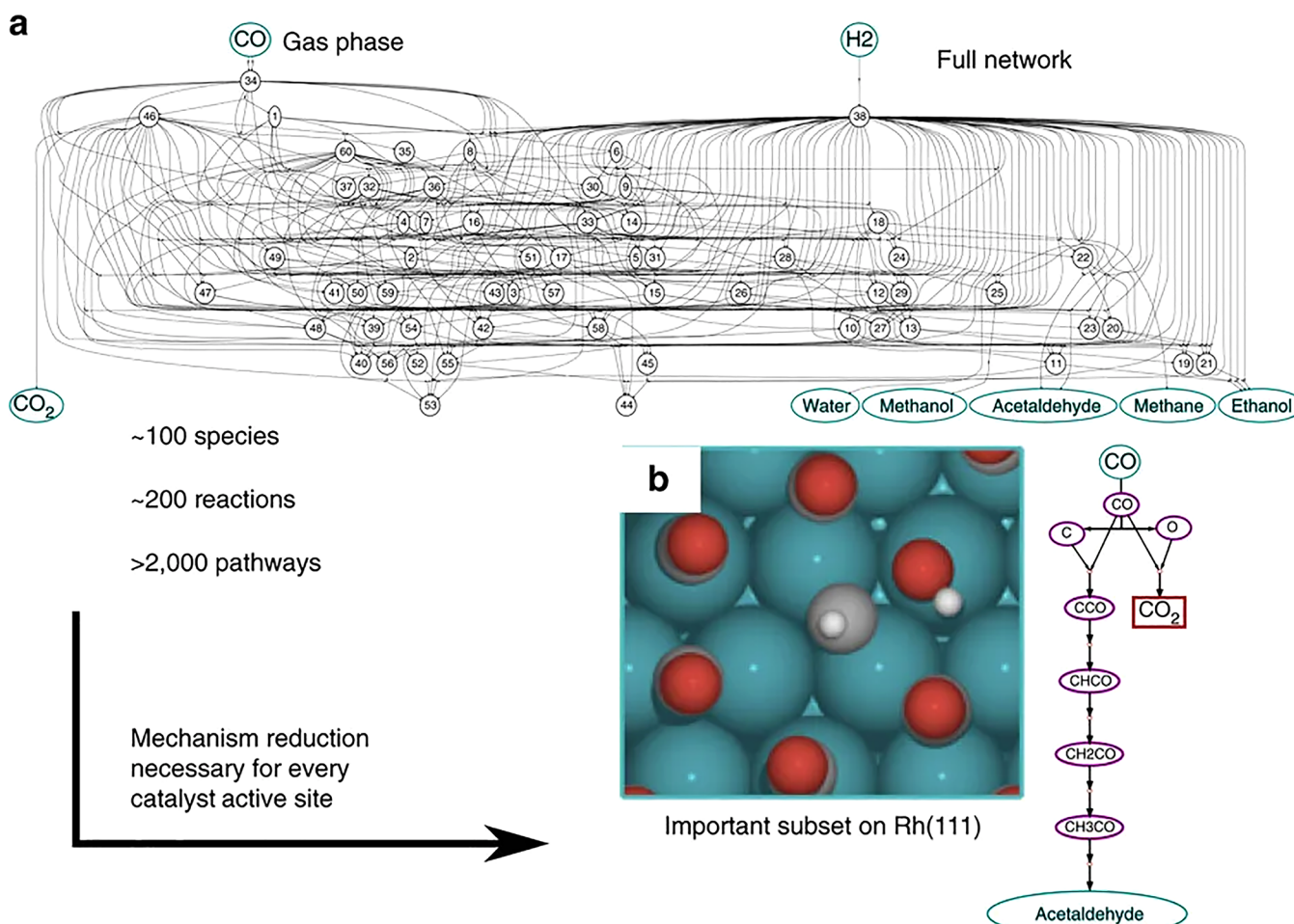


**Figure 2.** Example of an expansive and reduced reaction mechanism. (a) Reaction network for the conversion of syngas to carbon dioxide, water, methane, methanol, acetaldehyde, and ethanol. The reaction mechanism is quite expansive and consists of several hundred elementary reactions and thousands of possible reaction pathways. Modeling such an expansive mechanism is prohibitively expensive for catalyst design and discovery. (b) Reduced network for acetaldehyde production from syngas on Rh(111) confirmed by experimental techniques. Reproduced with permission from ref 45. Copyright 2017, Springer Nature under CC BY 4.0 [<http://creativecommons.org/licenses/by/4.0>].

include or exclude details based on experimental or computational evidence.<sup>22,46–53</sup> On the basis of semiempirical quantum mechanical calculations, the complex reaction mechanism shown in Figure 2a can be reduced to a simpler reaction mechanism shown in Figure 2b. Another method for reduction of complex reaction mechanisms is the so-called single event kinetic modeling, which has been extensively used in refining industry. In this method, the rate constant of each elementary reaction,  $k$ , is the product of a single-event rate constant,  $\tilde{k}$ , and the number of single events,  $n_e$ , that is,

$$k = n_e \tilde{k}$$

The single-event rate constant,  $\tilde{k}$ , only depends on the nature of the reactants and the type of reaction. Thus, the reaction rates are parametrized by a limited number of parameters. This approach reduces the number of independent parameters required to establish a kinetic model. A detailed analysis of this method is outside the scope of this review, and the interested reader is directed to recent reviews by Verstraete et al.<sup>54</sup> and Froment et al.<sup>55</sup>

Significant research efforts in development of plausible reaction mechanism have been undertaken, and various approaches for developing reaction mechanisms, particularly for complex systems, have been developed. These efforts include iterative approaches,<sup>56</sup> application of machine learning techniques,<sup>45,57</sup> and reaction mechanism generating software programs.<sup>58–63</sup>

In the iterative approach, a detailed initial reaction mechanism that includes an expansive set of elementary reactions is used. A microkinetic model is built using estimated parameters (discussed in section 2.5) to identify important elementary steps. These elementary reactions are then used to refine the initial reaction mechanism to obtain a plausible reaction mechanism on the catalyst surface. This approach is particularly useful for modeling of reactions that have been previously studied and for which a large data set of reaction energetics is available.<sup>64</sup> For cases where an initial reaction mechanism is not available, this approach is limited and in these cases a reaction mechanism generating program can be used instead. For example, for biomass upgrading, generating an expansive reaction mechanism can be challenging owing to the complexity of the number of intermediates and products that can be formed. In these cases, a rule-based reaction generator that employs structure–property relationship and other heuristics can be used to generate all possible elementary reactions.<sup>65</sup> These approaches are powerful as they provide a chemically meaningful reaction network without the additional requirement of running expensive quantum chemical calculations for reaction mechanism generation. Caution is required in the approach as the numbers of intermediates and elementary reaction generated increases with the size of the reactant molecules.<sup>66</sup> For example, the number of possible elementary reactions increases from 20 for the catalytic cracking of methanol to 500000 for catalytic cracking of hexanol.<sup>64</sup>

One possible solution to mitigate the increase in the number of intermediates and elementary reaction is to truncate the number of expansions with certain heuristics or rules;<sup>67</sup> however, such an approach runs the risk of missing reactions that might be kinetically significant.<sup>68</sup> Thus, the central challenge is to balance the need to include all elementary steps and the resources available for estimation of kinetic parameters to determine kinetically relevant elementary reactions. A strategy that has worked well for many reactions

is to generate an expansive reaction network using an automated reaction generator and then use approximate methods to determine kinetically relevant elementary reactions. Open-access software programs like NetGen (Broadbelt and Klein),<sup>66,69</sup> MECHEM (Valdés-Pérez),<sup>70–72</sup> RING (Daoutidis and Bhan),<sup>73,74</sup> and RMG-Cat (West and Green)<sup>60,75,76</sup> perform both of these tasks and are a good starting point for reaction mechanism generation for catalytic gas-phase reactions. A thorough discussion on the strengths and challenges of various reaction mechanism generators was recently published by Broadbelt et al.<sup>77</sup>

Liquid phase reactions present additional challenges as the solvent can impact the reaction mechanism by directly participating in the reaction; can influence the stability of certain intermediates and transition states thereby introducing additional reaction pathways or altering the relative importance of certain elementary reactions; can exhibit entropic confinement effects influencing the activation energy of certain elementary steps; and, can affect the reactant concentration by altering the solubility or solvation of various reactants or products. West et al. built a solvent sensitive reaction network by including linear solvation energy relationships and diffusion limitations in a reaction mechanism generator to model tetralin auto-oxidation.<sup>78</sup> A similar strategy may prove to be beneficial for liquid phase heterogeneous catalytic reactions such as upgrading of biomass derived molecules. An alternative approach, albeit computationally expensive, is to incorporate solvent effects in kinetic parameter estimation by employing either an implicit solvation model or explicit solvation models using empirical or fitted force field parameters.<sup>79</sup> For a comprehensive discussion on the application of computational techniques for investigating liquid phase phenomena to model homogeneous reactions, the reader is directed to a recent review by Mitchell et al.<sup>80</sup> and for the application of computational models at solid liquid interfaces the reader is directed to a recent review by Heyden et al.<sup>81</sup>

## 2.2. Stoichiometric Consistency

Once a reaction mechanism with  $n$  elementary reactions is formulated, the stoichiometric number, ' $\sigma_i$ ', for each step can be defined. The stoichiometric number is equal to the number of times each elementary step, as written, must be repeated to obtain the overall stoichiometric equation for the reaction. An example of a stoichiometrically consistent reaction mechanism is shown in Table 3.

For a reaction scheme with a single reaction path from reactants to products, the following identity is true at steady state:

**Table 3. Example of Stoichiometrically Consistent Reaction Mechanism**

step #	elementary reaction	$\sigma_i$
1	$N_2(g) + 2^* \rightleftharpoons 2N^*$	1
2	$H_2(g) + 2^* \rightleftharpoons 2H^*$	3
3	$N^* + H^* \rightleftharpoons NH^* + *$	2
4	$NH^* + H^* \rightleftharpoons NH_2^* + *$	2
5	$NH_2^* + H^* \rightleftharpoons NH_3^* + *$	2
6	$NH_3^* \rightleftharpoons NH_3(g) + *$	2
overall reaction	$N_2(g) + 3H_2(g) \rightleftharpoons 2NH_3(g)$	

$$r_{\text{overall}} = \frac{\vec{r}_i}{\sigma_i} = \frac{\vec{r}_i - \vec{r}_i}{\sigma_i} \quad (4)$$

where  $\vec{r}_i$ ,  $\vec{r}_i$ ,  $\sigma_i$  and  $r_i$  are the forward rate, reverse rate, stoichiometric number, and the total rate of the  $i$ th elementary step, and  $r_{\text{overall}}$  is the overall rate of the reaction. However, for reaction mechanisms with multiple parallel paths from reactant to products, the definition of stoichiometric numbers is not appropriate, and it is preferable to set up the kinetic model in terms of steady state relations for reaction intermediates (discussed in section 2.6).

### 2.3. Equilibrium Constant Estimation

Equilibrium constants for the  $i$ th elementary reaction are calculated from Gibbs free energy changes,  $\Delta G_i^o$  of the  $i$ th elementary step as:

$$K_{eq,i} = \exp\left(\frac{-\Delta G_i^o}{RT}\right) = \exp\left(\frac{\Delta S_i^o}{R}\right) \exp\left(\frac{-\Delta H_i^o}{RT}\right) \quad (5)$$

where  $K_{eq,i}$  is the equilibrium constant of the  $i$ th elementary reaction.  $\Delta H_i^o$  and  $\Delta S_i^o$  are the standard enthalpy and entropy change of the  $i$ th elementary reaction, respectively. The enthalpy and entropy changes are obtained from experimental data<sup>82–88</sup> or can be estimated by ab initio density functional theory (DFT) calculations,<sup>89–99</sup> the unity bond index-quadratic exponential potential (UBI-QEP) method,<sup>100–107</sup> or scaling relations.<sup>108–115</sup> The calculations for standard enthalpy change and entropy changes are discussed in Appendix I.

### 2.4. Thermodynamic Consistency

The nature of the catalyst affects the kinetics of the process but cannot change the thermodynamics of the overall reaction. Thus, it is important to ensure that any linear combination of elementary step that leads to the overall reaction is consistent with the overall reaction thermodynamics. Thus, the following relationship holds:

$$\sum_i \sigma_i \Delta H_i^o = \Delta H_{\text{overall}}^o \text{ and } \sum_i \sigma_i \Delta S_i^o = \Delta S_{\text{overall}}^o \quad (6)$$

Here,  $\sigma_i$  are the stoichiometric numbers of the linear combination of steps that lead to an overall stoichiometric reaction.  $\Delta H_{\text{overall}}^o$  and  $\Delta S_{\text{overall}}^o$  are the standard enthalpy and entropy change of the overall reaction. From eqs 5 and 6, the thermodynamic consistency of a reaction mechanism can be written in terms of the equilibrium constant of each elementary reaction:

$$\prod_i K_{i,eq}^{\sigma_i} = K_{\text{overall}} \quad (7)$$

where  $K_{\text{overall}}$  is the equilibrium constant of the overall reaction.

One strategy that ensures thermodynamic consistency is to relate the thermodynamic properties of adsorbed species to the known thermodynamics of gaseous species. For the cases where the adsorbed species does not necessarily desorb as a stable molecular species, the thermodynamic properties of the adsorbed species are related to the known thermodynamic properties of a gaseous radical or ion.<sup>116,117</sup> This strategy is shown graphically in Figure 3. However, when different sources are used to obtain adsorption enthalpies and entropies of reactive intermediates, achieving thermodynamic consistency can become challenging. Various methods have been implemented to ensure thermodynamic consistency in microkinetic analysis.<sup>118,119</sup> Vlachos et al. proposed a method wherein

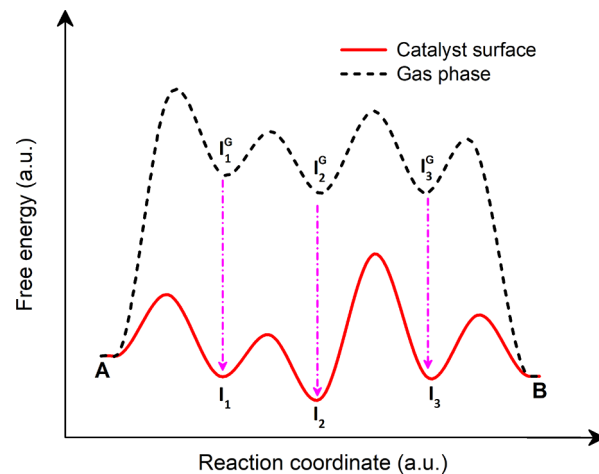


**Figure 3.** Free energy diagram showing thermodynamic consistency between gas-phase and catalyst surface.

the surface reaction properties are adjusted to achieve thermodynamic consistency.<sup>105,120</sup>

### 2.5. Rate Constant Estimation

Rate constants for each elementary reaction are required to obtain the reaction rate. Generally, the rate constants are estimated using transition state theory or collision theory.

**2.5.1. Collision Theory.** Rate constants for the adsorption and desorption of reactants and products can be estimated with collision theory. For the elementary adsorption reaction,



the rate of adsorption per unit area,  $r_A$ , is defined as:<sup>121</sup>

$$r_A = \sigma(T)f(\theta_r)F'' = \sigma(T)f(\theta_r)\frac{P_A}{\sqrt{2\pi m_A k_B T}} \quad (8)$$

where  $\sigma(T)$  is the probability that collision of a molecule with the clean surface leads to adsorption.  $\sigma(T)$  is the sticking coefficient and has a value between 0 and 1. The sticking coefficient can be expressed as:

$$\sigma(T) = \sigma^\circ \exp\left(\frac{-E_a}{R}\left(\frac{1}{T} - \frac{1}{T_o}\right)\right) \quad (9)$$

where  $E_a$  is the activation energy of adsorption, and  $\sigma^\circ$  is the sticking coefficient at a reference temperature,  $T_o$ .  $f(\theta_r)$  is a function of surface coverage and takes into account the available surface sites for adsorption. If the adsorption follows Langmuir isotherm model, then  $f(\theta_r)$  can be expressed as follows:

$$f(\theta_r) = \begin{cases} (1 - \theta_r) & \text{for non-dissociative adsorption} \\ (1 - \theta_r)^2 & \text{for dissociative adsorption} \end{cases} \quad (10)$$

where  $\theta_r$  is the reduced coverage and is the ratio of the surface coverage over the surface coverage at surface saturation. Despite the assumptions, the Langmuir isotherm describes many adsorption systems well. For cases where adsorbate–adsorbate interactions are important,  $f(\theta_r)$  does not decrease linearly with surface coverage, and various models have been proposed to account for the deviation from Langmuir adsorption model.<sup>122–125</sup> For a further detailed discussion on these models, we direct the reader to a report by Rudzinski et al.<sup>126</sup>

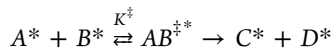
Since the rate of adsorption is:

$$r_A = \vec{k}P_A$$

the corresponding expression for the rate constant is:

$$\vec{k} = \frac{\sigma(T)f(\theta_r)}{\sqrt{2\pi m_A k_B T}} \quad (11)$$

**2.5.2. Transition State Theory.** Transition state theory assumes that an activated complex is formed from reactants before formation of the products. The activation complex is the molecular structure which lies at the saddle point in the potential energy landscape between the reactants and products. This activated complex is generally referred as the transition state. The critical assumption of transition state theory is that the transition state and the reactants of the elementary steps are in quasi-equilibrium as shown below:<sup>127</sup>



In this formulation, the reactants  $A^*$  and  $B^*$  form a transition state  $AB^{*\ddagger}$ , which is in equilibrium with the reactants. Using the equilibrium relation, the rate of forward reaction is obtained as:

$$\vec{r} = \vec{k}a_A a_B = \frac{k_B T}{h} \exp\left(\frac{\Delta S^{o\ddagger}}{R}\right) \exp\left(-\frac{\Delta H^{o\ddagger}}{RT}\right) a_A a_B \quad (12)$$

where  $k_B$  is the Boltzmann constant,  $h$  is the Plank's constant,  $a_A$  and  $a_B$  are the activities of the reactants  $A$  and  $B$ , respectively.  $\Delta H^{o\ddagger}$  and  $\Delta S^{o\ddagger}$  are the standard enthalpy change and standard entropy change for the formation of transition state from the reactants, respectively.  $\Delta H^{o\ddagger}$  is generally referred as the activation barrier/energy of the elementary reaction. The corresponding expression for rate constant is:

$$\vec{k} = \frac{k_B T}{h} \exp\left(\frac{\Delta S^{o\ddagger}}{R}\right) \exp\left(-\frac{\Delta H^{o\ddagger}}{RT}\right) \quad (13)$$

The rate constant for the reverse reaction is obtained by dividing the forward rate constant by the equilibrium constant of the elementary reaction:

$$\bar{k} = \frac{\vec{k}}{K_{eq}} \quad (14)$$

Both the forward and reverse rate constant can be estimated by transition state theory if the values for  $\Delta H^\circ$ ,  $\Delta S^\circ$ ,  $\Delta H^{o\ddagger}$ , and  $\Delta S^{o\ddagger}$  are available. Several approaches have been developed to estimate the relevant thermodynamic properties of adsorbed species and transition state of each elementary reaction. DFT methods are the most popular and have been used extensively in recent years.<sup>89,90,92–94,128–132</sup> The computational cost of DFT techniques increases dramatically with the size of molecules.<sup>133,134</sup> As a result, DFT techniques have been used for reaction consisting of moderate number of elementary steps and small molecules, such as water gas shift reaction, syngas upgrading, methane upgrading and electro-chemical reactions. It should be noted that DFT-derived parameters have some inherent error due to basis set truncation and extrapolation from 0 K (where DFT calculations are performed) to the reaction temperature.<sup>25</sup> Recently it was shown that errors in DFT-derived parameters can be significant when coarse integration grids are employed.<sup>135</sup> Additionally, DFT calculations are typically performed over single crystal surfaces which represent the most active sites for the reaction of interest, whereas the real catalyst is composed of various facets. As such, DFT-derived

parameters typically need adjustments to match experimental data. These parameter adjustments account for the error in DFT-derived parameters and are discussed in detail in section 2.8.

The UBI-QEP method, is an analytical method for determining  $\Delta H^\circ$  and  $\Delta H^{o\ddagger}$ . This method only requires gas-phase molecular bond energies and atomic heats of adsorption to estimate the molecular heats of adsorption and the activation barriers.<sup>136</sup> Generalized UBI-QEP efficiently calculates the heats of chemisorption of polyatomic molecules and activation barriers.<sup>101</sup> Owing to its simplicity, UBI-QEP can be applied to reaction networks with hundreds of steps and surface intermediates.<sup>136</sup> UBI-QEP has been used to model a range of reactions including water gas shift,<sup>100,107,137–140</sup> Fischer-Tropsch synthesis,<sup>106,136,141</sup> CO<sub>2</sub> hydrogenation,<sup>140,142</sup> and ammonia synthesis.<sup>143</sup> However, it should be noted that the entropic contribution to the rate constant is not calculated in UBI-QEP methods and as such the cases where entropic effects dominate, UBI-QEP should be used with caution.

Since the computational cost for calculating heat of adsorption and dissociation are much lower than that for calculation of activation energy, an effective approach to reduce computational cost for large reaction mechanisms is to calculate the heats of chemisorption and dissociation using DFT techniques, and to estimate the activation energies using the UBI-QEP method. A microkinetic model developed with these parameters can be used to identify kinetically important adsorbed species and transition states, and ab initio DFT methods can then be applied to a smaller subset of kinetically relevant adsorbates and elementary reactions. This approach dramatically reduces the overall computational cost, while maintaining the high accuracy predictions.<sup>64</sup>

## 2.6. Model Development

The law of mass action is used to determine the rate of each elementary reaction. For an elementary step  $i$ , the net rate of each elementary reaction is:

$$r_i = \vec{k}_i \prod_j P_j^{-\nu_{ij}} \prod_j \theta_j^{-\nu_{ij}} - \bar{k}_i \prod_j P_j^{\nu_{ij}} \prod_j \theta_j^{\nu_{ij}} = \sigma_i r \quad (15)$$

where  $\nu_{ij}$  is the stoichiometric coefficient of species  $j$  in the elementary step  $i$ . We use the convention that  $\nu_{ij} > 0$  if species  $j$  is a product of step  $i$ ,  $\nu_{ij} < 0$  if species  $j$  is a reactant of step  $i$ , and  $\nu_{ij} = 0$  if species  $j$  does not participate in step  $i$ . The net rate for each elementary step,  $r_i$ , is the product of the overall reaction rate,  $r$ , and the stoichiometric number,  $\sigma_i$ .

The rate of change of the surface coverage of a reaction intermediate is determined by the rate of production and consumption of the intermediate:

$$\frac{\partial \theta_j}{\partial t} = \sum_i \nu_{ij} r_i \quad (16)$$

An additional constraint is the conservation of surface sites, that is, the sum of all surface coverages must equal 1:

$$1 = \theta_* + \sum_j n_j \theta_j \quad (17)$$

where  $\theta_*$  is the concentration of free surface sites, and  $n_j$  is the number of surface sites occupied by the  $j$ th intermediate. For unidentate species,  $n_j = 1$ , for a bidentate species,  $n_j = 2$ , and so

forth. In cases where there is more than one type of active site, site balances are applied for all distinct active sites.<sup>27</sup> These equations, that is, eqs 15, 16, and 17, along with the proper material balance equation are solved numerically to obtain the surface coverages and the reaction rates of all elementary steps at steady state.

## 2.7. Numerical Solution Strategies

The rate constants of the elementary steps may span many orders of magnitude leading to a stiff set of differential equations. Thus, the set of coupled differential equations often cannot be solved by a standard ordinary differential equation (ODE) solver. The set of stiff differential equations can be solved by the backward difference method. Several readily available software such as MATLAB and Python have in-build methods for solving a set of stiff differential equations. For example, “ode15s” is an in-build solver in MATLAB that can be used to solve a set of stiff differential equations. However, there can arise cases where even the specialized solvers for stiff systems may fail. In these cases, it is possible to reduce the stiffness of the ODE system by reducing the rate constants of the elementary steps that are quasi-equilibrated, while ensuring that these elementary steps remain quasi-equilibrated and do not become kinetically significant.

Additionally, the governing equations for a steady-state plug flow reactor (PFR) is a differential-algebraic system, where the right-hand side of eq 16 becomes zero making that set of equation algebraic and the material balance is a differential equation. To solve differential-algebraic equations (DAE), a set of consistent initial guess is required. The initial surface coverages for a PFR can be estimated using a transient CSTR simulation with infinitesimal conversion. For a transient CSTR, eq 16 remains as a set of ODE and standard solvers can be used to obtain surface coverages until steady-state operation of the CSTR is achieved. Thus, a set of surface coverages are obtained that satisfies eq 16 at infinitesimal conversion. These surface coverages are then used as initial guesses to solve the system of DAE for steady-state PFR simulation.

## 2.8. Parameters Adjustments and Self-Consistency in Microkinetic Modeling

The DFT-derived parameters obtained by periodic boundary conditions have an inherent error between 0.1 and 0.2 eV.<sup>144,145</sup> The error in UBI-QEP estimated parameters can be higher than 0.2 eV. Moreover, DFT calculations are performed on a model surface, generally the most stable facet, whereas the metal and metal oxide nanoparticles expose different low-index facets depending on the size and shape of the nanoparticle.<sup>146–148</sup> Additionally, metal and metal oxide nanoparticles may undergo dynamic reshaping under reaction condition predominantly due to anisotropic changes in surface energies upon gas adsorption.<sup>149–152</sup> Moreover, the effects of the coadsorbed species on the energetics are rarely taken into account. Additionally, the DFT calculations are generally performed on a clean model surface; however, under operating conditions the catalyst surface is covered with intermediates which may affect the energetics of various elementary steps.<sup>153–155</sup> Furthermore, mean field microkinetic models assume perfect mixing wherein the spatial configuration of adsorbates is neglected leading to errors in energy estimation. Because of the above-mentioned shortcomings, microkinetic modeling can lead to limitations in design of catalytic material. However, microkinetic modeling in general has helped in understanding reaction trends across various catalysts, improving understanding of reaction mechanism and identifying elusive reaction intermediates and pathways.<sup>156–160</sup>

One simple way to take into account the heterogeneity of the catalyst surface is to obtain an average value of the energetics of reaction intermediates and transition states. Thus, the DFT parameters are often adjusted such that the predictions from microkinetic analysis matches experimental observations. Degree of rate control and degree of thermodynamic rate control (discussed in section 3.3) provide an efficient way to approach such adjustments. Surface intermediates and transition states that affect the net rate have large degree of rate control and must be adjusted to improve rate prediction from microkinetic analysis. This approach has potential for markedly improving rate predictions based on DFT with only moderate increases in computational costs.<sup>161,162</sup> Similar to the degree of rate control approach, a hierarchical multiscale approach was used by Mhadeshwar et al., that combines quantum mechanical DFT with semiempirical methods to improve predictive capabilities.<sup>163</sup> In this method, the initial model is developed with semiempirical methods to identify the important parameters, and only these parameters are then refined with the use of advanced computational method like DFT, thereby significantly reducing the computational cost.<sup>164</sup> Alternatively, the model parameters can be optimized by reducing the system of coupled ordinary differential equations to a set of nonlinear algebraic equations.<sup>165</sup> This approach is preferred over manual parameter optimization as it does not require prior knowledge, and a set of nonlinear algebraic equations can be easily solved with a nonlinear programming method. Also, this approach provides valuable information into the catalytic system.

In some cases large adjustments to parameters, greater than inherent DFT error, are required to accurately reproduce experimentally measured apparent activation energies and reaction orders.<sup>165</sup> The catalytic activity may depend on the surface coverages by the various adsorbates. The importance of surface coverages effects has been demonstrated by studying the transient response of acetone hydrogenation on supported Pt catalysts, where the adsorption energy of the surface intermediates was shown to increase with decreasing surface coverage.<sup>166</sup> Another notable example of this phenomenon is the oxidation of NO over Pt catalysts.<sup>167–169</sup> At low oxygen coverage, adsorbed O\* binds strongly leading to low catalytic activity; however, with increasing surface coverage of oxygen, the adsorption energy of oxygen decreases leading to increased catalytic activity.<sup>169</sup> In these cases, it is important to include coverage-dependent energetics in microkinetic modeling. Generally, it is instructive to include surface coverage effects for reactions where the apparent activation energy and order of the reaction with respect to the reactants and products change as a function of reactant/product concentration or as a function of conversion.<sup>170</sup> It has been shown that adsorbate–adsorbate interactions do not affect the position of the most-optimal catalyst on the activity volcano curve (volcano plots are discussed in section 4) as the optimal catalyst operates in the regime wherein the catalyst does not bind the reactant strongly or weakly, but adsorbate–adsorbate interactions can significantly influence the selectivity of the catalyst.<sup>171</sup> Several studies have incorporated adsorbate interactions by expressing the energetics of important surface species as a function of surface coverages.<sup>171–174</sup> For example, these effects can be included by dynamically including coverage effects using the Bragg-Williams approximation, and this approach was employed to describe experimentally observed acetone hydrogenation activity over a wide range of reaction conditions.<sup>166</sup> An iterative approach was used by Mavrikakis et al. to develop a self-consistent

microkinetic model for formic acid decomposition.<sup>175</sup> While these models include the coverage dependent energetics, they ignore spatial correlations. A cluster expansion framework has been utilized to incorporate spatial lattice interactions into mean-field microkinetic models.<sup>176–180</sup> Such models are computationally expensive and more complicated to solve than mean field microkinetic models. A detailed discussion on advances in parameter estimation for accurate model predictions was presented in a recent article by Matera et al.<sup>181</sup>

### 3. ANALYSIS AFTER MODEL DEVELOPMENT

The goal of performing microkinetics is to develop catalytic material with improved performance. Determining the key kinetic parameters that control the performance of the catalytic material enables the researcher to design better material with improved properties. Next, we outline methods to analyze the results of the model and draw meaningful conclusions.

#### 3.1. Reversibility of Elementary Steps and Its Properties

One simple yet extremely insightful property is the reversibility. The reversibility of an elementary step,  $z_i$ , is defined as the ratio of the reverse rate to the forward rate:<sup>182</sup>

$$z_i = \frac{\vec{r}_i}{\vec{r}_i} \quad (18)$$

The numerical value of the reversibility is equal to 0 for an irreversible step and approaches 1 for a quasi-equilibrated step. The overall reversibility of the reaction is the product of the reversibility of the elementary steps raised to the stoichiometric number for that step:

$$z_{\text{total}} = \prod_i z_i^{\sigma_i} \quad (19)$$

where  $z_{\text{total}}$  is the total reversibility and is equal to the approach to equilibrium,  $\beta$  (eq 3). The following important conclusions can be drawn using the magnitude of reversibility:<sup>183,184</sup>

- The kinetic parameters associated with the quasi-equilibrated steps ( $z_i = 1$ ) have little to no effect on the overall rate of the reaction.
- All elementary reaction following an irreversible elementary step ( $z_i = 0$ ) have no effect on the overall rate of the reaction.
- Kinetic parameters associated with elementary steps that do not follow an irreversible step and has intermediate reversibility ( $0 < z_i < 1$ ) influence the overall rate of the reaction.

The reaction mechanism has a single rate-determining step if the reversibilities of all but one step, are equal to unity. For reaction mechanisms with multiple rate controlling steps, the reversibility of rate controlling steps is between 0 and 1.

#### 3.2. Sensitivity Analysis

A useful tool in analysis of the microkinetic model is sensitivity analysis. Sensitivity,  $S_p$ , of an elementary step is defined as relative increase in the overall rate per relative increase in the rate constant for step  $i$ , holding all other rate constants as constant:

$$s_i = \frac{k_i}{r} \left( \frac{\partial r}{\partial k_i} \right) \Bigg|_{k_j \neq i} \quad (20)$$

The magnitude of sensitivity determines the influence of the rate constant on the overall reaction rate. A positive value indicates

that increasing the corresponding rate constant will increase the overall rate, whereas, a negative value of sensitivity indicates the opposite. Additionally, it has been shown that the sensitivity of the reverse reaction is equal to the negative of the product of the reversibility and the sensitivity of the forward reaction:<sup>182</sup>

$$s_{-i} = -z_i s_i \quad (21)$$

This result implies that the sensitivity of the overall rate to the reverse rate constant of an elementary reaction depends on the reversibility of that reaction. For example, for an irreversible elementary reaction ( $z_i = 0$ ), the sensitivity of the overall rate to the reverse rate constant is equal to zero and for an equilibrated elementary reaction the sensitivity of the reverse rate constant to the overall rate is equal to the negative value of the sensitivity of the overall rate to the forward rate constant. Furthermore, the sensitivity of the overall rate to the forward rate constant for an elementary reaction is always proportional to the reversibility of the preceding step that produces the reaction intermediate in the current step:

$$s_{i+1} \propto z_i s_i \quad (22)$$

The proportionality constant depends on the stoichiometric coefficients for the formation and consumption of the reactive intermediates.<sup>185</sup> Using sensitivity analysis, one can identify key transition states that control the rate of the overall reaction.

Sensitivity analysis has been used to determine rate-determining steps for various reaction mechanisms.<sup>186–188</sup> A notable example is the partial oxidation of ethylene to ethyne oxide. Linic and Bartea<sup>186</sup> used sensitivity analyses to determine that the dissociative adsorption of oxygen and addition of weakly adsorbed ethylene to the oxygen-covered sites were the rate determining elementary reactions for partial oxidation of ethylene over a supported silver catalyst.

#### 3.3. Degree of Rate Control

Campbell suggested that the importance of a particular transition state toward the overall reaction rate can be ascertained by changing the energy of that particular transition state while keeping the energy of all other reaction intermediates and transition state constant (see Figure 4). It should be noted that when the energy of the transition state of an elementary reaction is changed, both the forward and the reverse rate constant are changed simultaneously, however, the equilibrium constant remains unchanged.<sup>183,189,190</sup> The degree of rate control for step  $i$ , is equal to:

$$X_{RC,i} = \frac{\vec{k}_i}{r} \left( \frac{\partial r}{\partial \vec{k}_i} \right) \Bigg|_{K_{i,\text{eq}}, k_{j \neq i}} = \left( \frac{\partial \ln r}{\partial \ln \vec{k}_i} \right) \Bigg|_{K_{i,\text{eq}}, k_{j \neq i}} \quad (23)$$

where the equilibrium constant for step  $i$  and all other rate constants are held constant. The magnitude of  $X_{RC,i}$  determines the influence of the transition state of step  $i$  on the overall reaction rate. A negative value indicates that increasing the corresponding forward rate constant will decrease the overall rate, while a positive value indicates that increasing the corresponding forward rate constant will increase the overall rate. Additionally, for any reaction scheme with a single overall reaction, that is, byproduct formation is not included in the reaction mechanism, the degree of rate control is conserved,<sup>182,185</sup> that is,

$$\sum_i X_{RC,i} = 1 \quad (24)$$

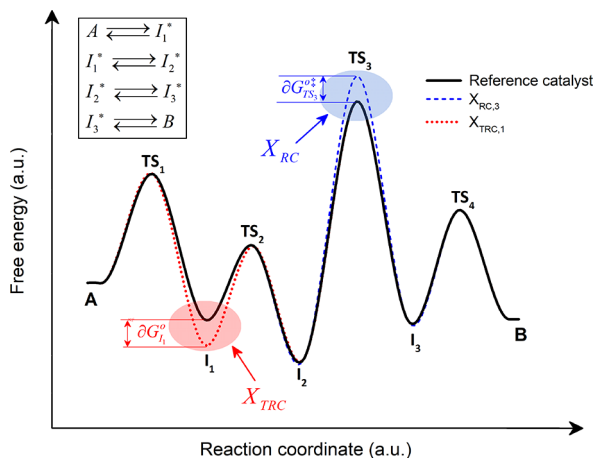


**Figure 4.** Schematic standard state free energy diagram for a hypothetical reaction  $A \rightleftharpoons B$ , showing an incremental increase in the standard state free energy of transition state of step 3,  $TS_3$ . This defines the degree of rate control for that step ( $X_{RC,3}$ ). Also showing an incremental decrease in the standard state free energy of reaction intermediate,  $I_1$ . This defines the thermodynamic degree of rate control for that intermediate.

The magnitude of the degree of rate control of each elementary reaction reflects the relative contribution of the elementary reaction in controlling the rate of the overall reaction. For a reaction mechanism with a single rate-determining step, the degree of rate control for that step is equal to 1. Alternatively, the degree of rate control of a reaction can be written in terms of the standard state Gibbs free energies:

$$X_{RC,i} = \frac{RT}{r} \left( \frac{\partial r}{\partial (-G_i^{\circ\ddagger})} \right) \Bigg|_{G_j^{\circ\ddagger}} = \left( \frac{\partial \ln r}{\partial (-G_i^{\circ\ddagger}/RT)} \right) \Bigg|_{G_j^{\circ\ddagger}} \quad (25)$$

where the Gibbs free energies of all transition states and reaction intermediates except the Gibbs free energy of the transition state of the  $i$ th step,  $G_i^{\circ\ddagger}$ , are held constant. The above analysis can be extended to stable reaction intermediates as well (see Figure 4). Campbell<sup>190</sup> termed the degree of rate control by reactive intermediates as thermodynamic degree of rate control. For a stable reaction intermediate,  $j$ , the thermodynamic degree of rate control is:

$$X_{TRC,j} = \frac{1}{r} \left( \frac{\partial r}{\partial (-G_j^{\circ}/RT)} \right) \Bigg|_{G_k^{\circ\ddagger}, G_i^{\circ}} \quad (26)$$

where the Gibbs free energies of all transition states and reaction intermediates except the reaction intermediate of interest,  $G_i^{\circ}$ , are held constant.

Degree of rate control and the thermodynamic degree of rate control have been used extensively in the literature to identify rate controlling reactions and intermediates.<sup>18,156,174,190–193</sup> A thorough discussion of the utilization of degree of rate control in heterogeneous catalysis applications was recently presented by Campbell.<sup>194</sup>

The apparent activation energy of a reaction is estimated by calculating the reaction rate as a function of reaction temperature using the Arrhenius equation. For a generalized reaction mechanism with two rate-determining steps, it has been shown<sup>170</sup> that the apparent activation energy is related to the

degree of rate control of the rate-determining steps and the surface coverage of the most abundant surface intermediate as:

$$E_{app} = X_{RC,1} E_1^{\ddagger} + X_{RC,2} E_2^{\ddagger} - n \theta_{MASI} H_{MASI}^g \quad (27)$$

where  $E_1^{\ddagger}$  and  $E_2^{\ddagger}$  are enthalpy of formation of the transition state of the rate-determining steps from the gas phase reactants,  $H_{MASI}^g$  is the enthalpy of formation of MASI from the gas phase reactants and products,  $\theta_{MASI}$  is the surface coverage of the most abundant surface intermediate, and  $n$  is the number of surface sites involved in the rate-determining step. An inherent assumption in eq 27 is that the numbers of surface sites involved in the rate-determining steps are equal. This behavior is due to the assumption made in determining the overall reaction rate in maximum rate analysis (see section 6). Thus, eq 27 is true for cases where there is only one rate-determining step or cases where the numbers of surface sites in the rate-determining steps are equal. However, this assumption may not be true for all reactions and caution is advised while using eq 27.

The following example shows the application of eq 27 for  $\text{CO}_2$  hydrogenation over  $\text{Cu}(211)$  to form methanol. A simplified reaction mechanism consisting of 8 elementary steps was proposed by Studt et al.<sup>195</sup> to explain experimental rate measurements. Mao et al. performed microkinetic modeling and determined the surface coverages and degrees of rate control for the proposed reaction mechanism for  $\text{CO}_2$  hydrogenation to methanol.<sup>196</sup> They determined that  $\text{HCOO}^*$  was the MASI with the surface coverage of 0.984 and the enthalpy of formation of MASI from the gas phase  $\text{CO}_2$  and  $\text{H}_2$  was  $-98.33 \text{ kJ/mol}$ , and the third hydrogenation step is the only rate-determining reaction with the enthalpy of formation of the transition state from the gas phase  $\text{CO}_2$  and  $\text{H}_2$  of  $23.45 \text{ kJ/mol}$ . Under these conditions, the apparent activation energy from eq 27 is:

$$\begin{aligned} E_{app} &= 1 \times 23.45 - 2 \times 0.984 \times (-98.33) \\ &= 216.96 \text{ kJ/mol} \end{aligned}$$

Since the rate-determining step involves two surface sites,  $n$  equals 2. The predicted value of  $\sim 217 \text{ kJ/mol}$  from eq 27 is in good agreement with the activation energy of  $220 \text{ kJ/mol}$  obtained from solving the full microkinetic model.

Campbell et al.<sup>196</sup> further generalized the results in eq 27 and proved that the apparent activation is the sum of the standard-state enthalpies of all species (including all intermediates and transition states) that appear in the reaction pathway, each weighted by its degree of rate control, that is,

$$E_{app} = RT + \sum_i X_i H_i^o \quad (28)$$

where  $X_i$  is the degree of rate control and  $H_i^o$  is the enthalpy of  $i$ th reaction species relative to that of the reactants (i.e., reactants are considered as the zero-energy reference state). Dumesic et al.<sup>170</sup> demonstrated the applicability of eq 27 in ammonia synthesis and Campbell et al.<sup>196</sup> demonstrated the applicability of eq 28 in methanol synthesis through  $\text{CO}_2$  hydrogenation. Campbell et al. have also discussed the limitations of several other equations proposed in the literature for estimation of apparent activation energy using degree of rate control.<sup>196</sup>

Additionally, the degree of rate control analysis can be used to perform quantitative analysis of the magnitude of the kinetic isotope effect (KIE) in reaction mechanisms. Campbell et al.<sup>197</sup> proved that the KIE for a reaction mechanism is the product of the exponential of standard-state free-energy difference between

the two isotopes, each weighted by its degree of rate control, that is,

$$KIE = \prod_i \exp \left[ -X_i \frac{G_{i,H}^o - G_{i,D}^o}{RT} \right] \quad (29)$$

where  $G_{i,H}^o - G_{i,D}^o$  is the standard state free energy difference between the two isotopes for the  $i$ th species in the reaction mechanism. It should be noted that in eq 29, the product is over all species in the reaction mechanism, including the reactants, the products, the intermediates, and the transition states.

### 3.4. Selectivity and Degree of Selectivity Control

For reaction schemes leading to multiple reaction products, the selectivity to a desired product is an important criterion. The selectivity,  $S$ , is defined as the ratio of the rate of production of the desired product over the rate of consumption of the reactant. Alternatively, selectivity can also be obtained as the ratio of the rate of production of the desired product over the sum of the rate of production of all products, that is,

$$S_i = \frac{r_{P,i}}{r_R} = \frac{r_{P,i}}{\sum_j r_{P,j}} \quad (30)$$

where  $S_i$  is the selectivity to the desired product,  $i$ ,  $r_{P,i}$  is the rate of production of desired product,  $i$ , and  $r_R$  is the rate of consumption of the reactants, which is equal to the sum of the rate of production of all products. Thus, the selectivity to any desired product can be estimated from the results of the microkinetic model. Similar to the degree of rate control, the degree of selectivity control which identifies the selectivity controlling steps was defined by Stegelmann et al.<sup>21,190,193</sup> as:

$$X_{SC,i} = \frac{\vec{k}_i}{r} \left( \frac{\partial S}{\partial \vec{k}_i} \right) \Bigg|_{K_{i,eq}, k_{j \neq i}} = \left( \frac{\partial \ln S}{\partial \ln \vec{k}_i} \right) \Bigg|_{K_{i,eq}, k_{j \neq i}} \quad (31)$$

where  $S$  is the selectivity of the overall reaction to a desired product. As an example,  $X_{SC,i}$  was used to identify the selectivity controlling steps for ethylene oxide production during partial oxidation of ethylene, and it was determined that the selectivity was dependent on the relative rates of ring closure of oxametallacycle to form ethylene oxide and H-abstraction from oxametallacycle to form carbon dioxide.<sup>21,193</sup>

## 4. BRØNSTED–EVANS–POLANYI AND SCALING CORRELATIONS

A qualitative concept in heterogeneous catalysis is the Sabatier principle, which states that the highest reaction rate is achieved for surfaces where intermediates bind to the catalyst surface with optimal bond strength.<sup>198</sup> Surfaces on which the intermediates bind weakly result in poor activation of reactants, and conversely surfaces on which intermediates bind strongly result in high coverage and thus limited availability of free sites for reaction. This balance leads to a volcano relationship between the bond strength of intermediates and the activity of the catalyst as shown in Figure 5.

For quantitative analyses to explore the Sabatier principle, a descriptor is required that can describe the bond strength between the intermediates and the catalyst surface. Bulk properties of the catalyst have been used as descriptors, such as the heat of formation of the metal oxide,<sup>199</sup> d-band center,<sup>200,201</sup> work function, excess Bader charge on the adsorbates, intermediate number of d-electrons in the valence

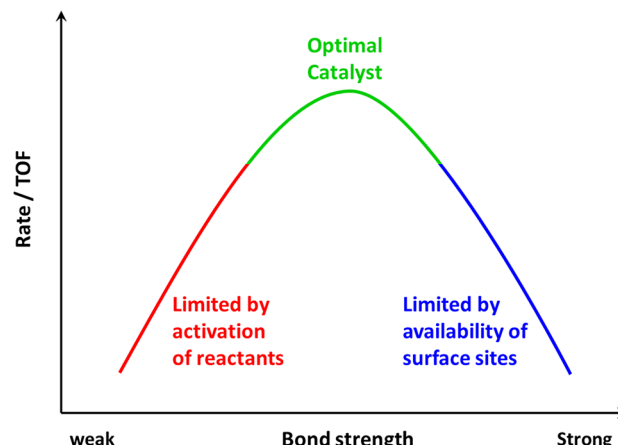


Figure 5. Schematic representation of the Sabatier principle.

band.<sup>202</sup> Importantly, it has been found that for several simple surface reactions, the chemisorption energy is a good descriptor.<sup>203</sup>

In 1938, Evans and Polanyi demonstrated that for a homologous reaction series (i.e., reactions with similar transition states) the activation energy of a reaction,  $E_a$ , is proportional to the heat of reaction,  $\Delta E$ .<sup>204</sup> Such relationships are generally referred as Brønsted–Evans–Polanyi or Bell–Evans–Polanyi (BEP) correlations:

$$E_a = \alpha \Delta E + \beta \quad (32)$$

where  $\alpha$  and  $\beta$  are constants.

Nørskov et al. showed that BEP relations are universal in heterogeneous catalysis.<sup>203</sup> BEP correlations are powerful tools in determining the properties of optimal catalysts because the major computational cost in performing microkinetic modeling is the energy calculation for transition states. Using BEP relations, the activation energy can be obtained from the heat of reaction calculations, which are computationally less demanding. Thus, BEP relations reduce the computational resources required for establishing trends in reactivity among the different transition metals. As such, BEP correlations have been used extensively in the literature to identify promising catalysts for various reactions.<sup>22,198,203,205–225</sup> An example of a BEP relation is shown in Figure 6 for C–C, C–O, C–H, and O–H dissociation reactions. It is evident from Figure 6 that the energy of the transition state is correlated with the enthalpy of the dissociation reaction. It should be noted that the zero-point energy calculations have significant effect on correlation parameters and must be carefully evaluated.<sup>210</sup>

Universal BEP correlations provide a convenient way to explore trends in catalytic reactions. To reduce computational cost, a BEP correlation is generated for a class of reaction. For example, Figure 6 shows the BEP correlation for C–H bond cleavage and this correlation can be used for various reactions involving C–H bond activation. However, care must be taken in utilizing these relations for different reactions, as a central point in development of BEP correlations is that the correlations are valid for homologous reaction series. Vlachos et al. showed that the maximum absolute error in application of BEP correlations can be significantly reduced when the reactions are classified into homologous series based on the similarity of reaction families.<sup>218,226</sup> Thus, application of BEP correlations must be carefully applied after examining the structure of the adsorbed molecule and the transition state. For example, the BEP

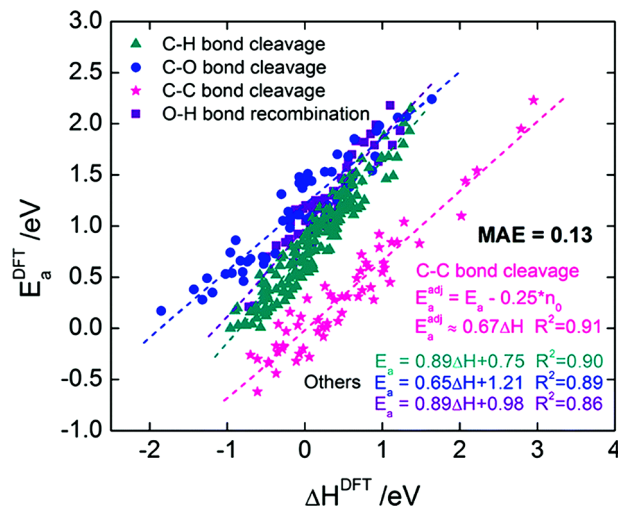


**Figure 6.** (a) Universal BEP relationship between activation energy and the enthalpy of reaction obtained from DFT calculations for the C–O, C–C, C–H, and O–H bond cleavage reactions on a variety of transition metal surfaces. Reproduced from ref 222. Copyright 2019 PCCP Owner Societies.

correlation for C–H bond scission of small hydrocarbon molecules can be used to explore trends in dehydrogenation of biomass derived furans, as the adsorbed state and the transition state for these elementary reactions are similar.<sup>218</sup> On the contrary, the BEP correlation for O–H bond dissociation in small molecules like glycerol is different than O–H bond dissociation in biomass derived large molecules like guaiacol due to the differences in the structure of the transition states of these molecules.<sup>227,228</sup> Thus, it is important to apply BEP correlations with caution.

While BEP relations greatly reduce the cost of computational resources, the chemisorption energy of all the surface intermediates must still be calculated. Since the chemisorption energies of all the intermediates are treated as independent parameters, drawing conclusion from a model with many independent variables is a difficult task. Thus, a considerable reduction in the number of independent parameters is required. The solution to this problem lies in the generality of the scaling relations, which states that the change in the adsorption/binding energy of an intermediate from one catalyst surface to another is linearly related to the change in the adsorption energy of a descriptor with similar binding to the surface of the catalyst:

$$\Delta E_{\text{intermediate}} = \gamma \Delta E_{\text{descriptor}} + \delta \quad (33)$$

where  $\gamma$  and  $\delta$  are constants. Figure 7 shows that a linear relationship exists between the chemisorption energies of all the intermediates in formic acid decomposition. Specifically, the chemisorption energy of each intermediate can be written as a linear function of the binding energy of either CO or OH. Thus, with the application of scaling relations, the total number of variables in a microkinetic model can be reduced to a few independent variables (generally two descriptors are sufficient). It is observed from Figures 6 and 7 that there is an uncertainty associated with both BEP and scaling correlations. As such, it is expected that these uncertainties will be propagated in model prediction. It was recently shown that the uncertainty in linear relationships, and not BEP correlations, are the dominant contributor to the uncertainty in model predictions.<sup>229,230</sup> It was also shown that the position of the most optimal catalyst can be

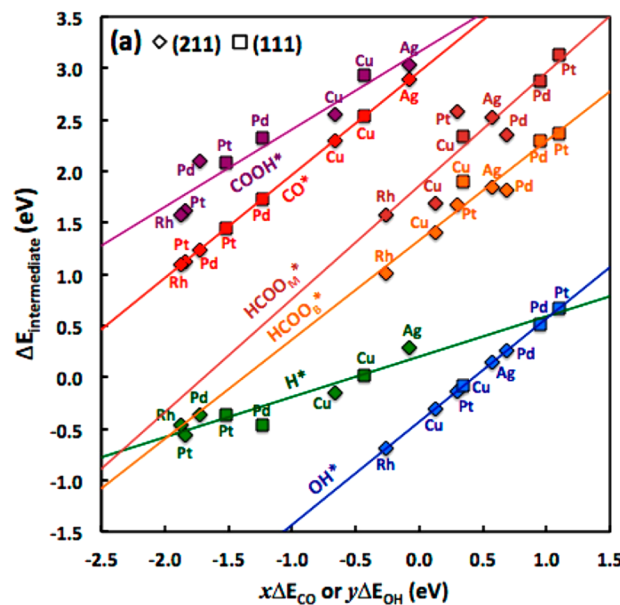


**Figure 7.** Scaling relations between the adsorption energies of the reaction intermediates of formic acid decomposition as a function of the adsorption energies of CO or OH. All adsorptions energies were calculated using DFT calculations. Reprinted with permission from ref 22. Copyright 2014 American Chemical Society.

estimated within 0.1 eV (see Figure 8), that is, the uncertainty is less than 10%.<sup>229</sup> Thus, these correlations can be used to guide the optimization of catalyst properties as shown in the example below.

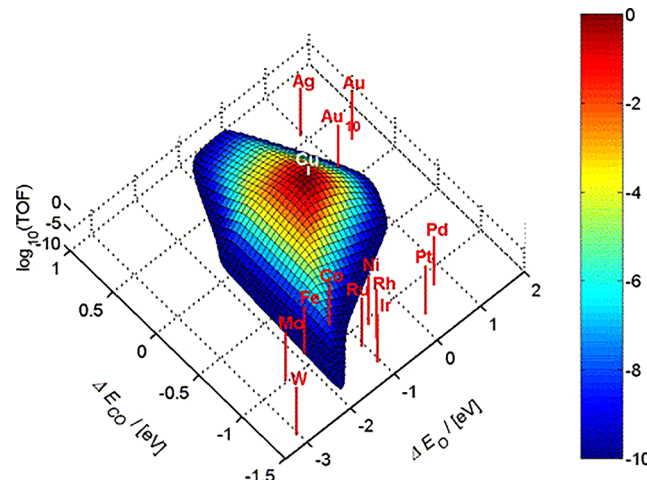


**Figure 8.** Theoretical activity volcano plot for the water gas shift reaction. The turnover frequency (TOF) is plotted as a function of the CO and O adsorption energies. The chemisorption energies for all metals are relative to the copper. Reprinted with permission from ref 41. Copyright 2005 Elsevier.

As an example, consider the water-gas shift reaction, which is an important process for the production of hydrogen. Schumacher et al.,<sup>41</sup> studied the redox pathway for water gas shift reaction. The binding energies of all reaction intermediates of the water gas shift reaction were shown to scale linearly with the binding energy of either adsorbed oxygen or carbon-monoxide. A microkinetic model was built to predict the turnover rate as a function of the binding energy of oxygen and

carbon, as shown in Figure 8. Cu is close to the optimal catalyst, as Cu moderately binds both O\* and CO\*. Precious metals like Pt and Rh show poor performance due to strong CO adsorption, whereas noble metal like Au and Ag show poor performance due to weak binding of both CO\* and O\*.

BEP relations and scaling relations have proven to be useful in determining the volcano plots, but this approach requires linear relationships between the energy of the descriptor and all reaction intermediates and transition states. Campbell et al. showed that volcano plots can be obtained by considering the energies of only those species that have significant degree of rate control.<sup>231</sup> In this method, a microkinetic model is developed for a reference catalyst and the values of  $X_{RC}$  and  $X_{TRC}$  are calculated for all species. A volcano curve is obtained by considering only the species with high degree of rate control. This procedure was employed for the analysis of methane steam reforming using Rh(211) as the reference catalyst and was shown to be computationally faster than the complete BEP analysis.<sup>231</sup> However, this approach is accurate only for the metals that are similar to the reference metal, as the degree of rate control can significantly change for a metal that is dissimilar to the reference metal.

It should be noted that the BEP and scaling relations reported in literature are generally obtained at low adsorbate coverage. Kitchin et al.<sup>232</sup> showed that the scaling correlation weakens with increasing surface coverage. Additionally, the correlation may reverse at high surface coverage. Thus, precautions are warranted when BEP and scaling relations are used for reactions with high surface coverage.

#### 4.1. Scaled Degree of Rate Control

The degree of rate control identifies the key elementary reactions that control the rate of the reaction; however, it is not generally possible to independently change the energetics of a species since energetics of various species are correlated through the BEP and scaling correlations. This limits the usefulness of the degree of rate control to the identification of the rate-determining steps. Avanesian and Christopher introduced the concept of scaled degree of rate control that explicitly incorporates BEP correlations into the degree of rate control analysis.<sup>233</sup> The scaled degree of rate control,  $X_{S-RC,i}$ , for step  $i$ , is defined as:

$$X_{S-RC,i} = \left( \frac{\partial \ln r}{\partial (-H_i^{\ddagger}/RT)} \right)_{H_j^o} \times \frac{dH_i^{\ddagger}}{dH_x^o} = X_{RC,i} \varepsilon_i \quad (34)$$

where  $H_i^{\ddagger}$  is the standard-state enthalpy of the transition state of step  $i$ ,  $H_x^o$  is the enthalpy of the descriptor, and  $\varepsilon_i$  is a scaling factor, which indicates the correlation between the energy of the transition state of step  $i$  and the descriptor. This concept was used to identify the rate controlling elementary reaction for CO<sub>2</sub> reduction.<sup>233</sup> Using the degree of rate control, it was determined that the dissociation of CHO\* was the key rate-determining step for CH<sub>4</sub> formation and desorption of CO\* was the key rate limiting step for the formation of CO. However, using the scaled degree of rate control analysis a different conclusion was reached. It was determined that the desorption of CO\* plays a less significant role when parametric correlations are considered (see Figure 9). Here, it is important to realize that only one descriptor was used in this analysis, and, poor correlation exists between the adsorption energies of dissimilar adsorbates. Specifically for CO<sub>2</sub> reduction, the correlation is weak between the binding energies of adsorbates with metal-C bonding (like

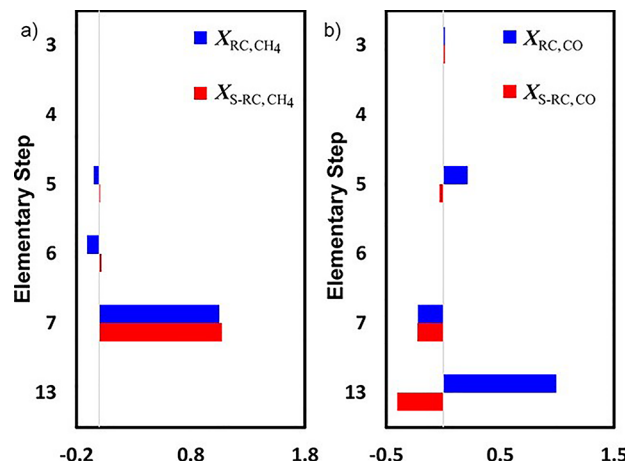


**Figure 9.** Comparison between the calculated degree of rate control,  $X_{RC}$ , and scaled degree of rate control,  $X_{S-RC}$  for (a) CH<sub>4</sub> formation and (b) CO formation during CO<sub>2</sub> reduction by H<sub>2</sub>. Reprinted with permission from ref 233. Copyright 2016 American Chemical Society.

CH\*) and adsorbates with metal-O bonding (like OH\*), and as such the conclusions drawn for CO<sub>2</sub> reduction using scaled degree of rate control are only reasonable for the series of late transition metals (where a reasonable correlation exists). Therefore, scaled degree of rate control must be used with great caution.

## 5. MACHINE LEARNING IN MICROKINETIC MODELING

Machine learning approaches, like artificial neural networks, have been used for catalyst development. Early studies focused on correlating the catalyst performance and the physiochemical properties of the catalyst.<sup>234,235</sup> Recently, machine learning algorithms have been combined with DFT calculations for accurate and fast screening of the vast catalyst space.<sup>236,237</sup> For example, Asahi et al. used machine learning algorithms to predict the activity of alloy nanoparticles for the direct decomposition of NO over RhAu bimetallic catalysts with significantly reduced computational expense.<sup>236</sup> Similarly, a combined DFT and neural network (NN) approach was used to study Ni–Ga bimetallic catalysts for CO<sub>2</sub> electro-reduction. The combined DFT-NN approach reduced the required number of DFT calculation by at least an order of magnitude.<sup>237</sup>

Machine learning algorithms have also been used with large experimental data set to guide catalyst formulation. Zavala et al. used neural network analysis on a comprehensive data set for the water-gas-shift reaction to identify new catalyst formulations that exceed the performance of the catalysts included in the data set.<sup>238</sup>

Another important avenue for machine learning tools is in the identification of proper descriptors that can be used to efficiently screen large catalyst space. A descriptor that does not require quantum mechanical calculations would accelerate catalyst prediction and screening. Noh et al. used machine learning methods to identify that the d-band width and the electronegativity of component metals can be used as descriptors to calculate the CO adsorption energy on alloy surfaces.<sup>239</sup> Using this model, they identified Cu<sub>3</sub>Y@Cu as a cost-effective catalyst for electrochemical CO<sub>2</sub> reduction with significantly reduced computational cost.

Finally, machine learning is being used to develop exchange and correlation functional that are trained on DFT-derived data. These functionals can increase the computational efficiency by

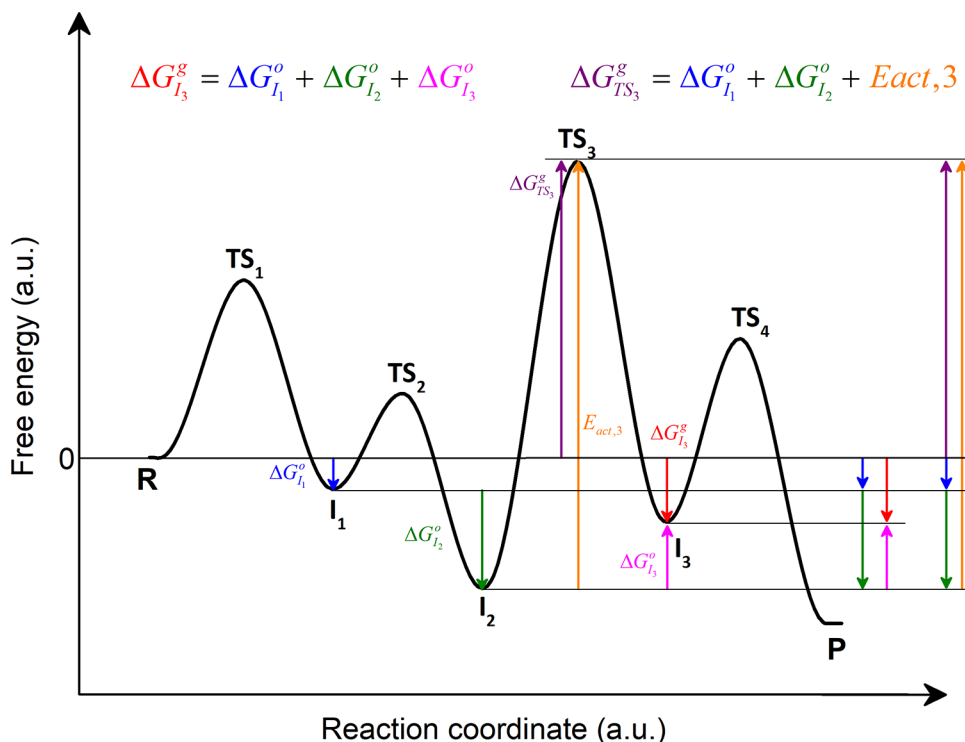


**Figure 10.** Free energy diagram showing the relationship between the free energy change for the formation of intermediates directly from gas phase and the free energy change for the formation of intermediates on the catalyst surface. Similar relationship for transition state is also illustrated.

several orders of magnitude without losing accuracy compared to DFT methods.<sup>240,241</sup> The enhanced performance can potentially help to perform detailed quantum mechanical calculation on large molecules.<sup>242</sup>

We have provided here a brief overview of the potential of machine learning tools in catalyst development. A detailed discussion on various machine learning tools and their application is outside the scope of this review and we refer the reader to a recent review by Goldsmith et al.<sup>243</sup>

## 6. MAXIMUM RATE ANALYSIS

Microkinetic modeling is a powerful technique for identification of prominent reaction pathways and providing important information for design of new catalytic materials. However, it requires the numerical solution of coupled stiff differential equations. Moreover, based on the reactor model, the set of equations may lead to differential-algebraic equation (DEA) of index greater than one, requiring index reduction and a consistent set of initial conditions. Providing a consistent set of surface coverages that satisfies the residual equations is challenging. However, as was outlined earlier, not all reaction steps are rate-determining steps, and reaction steps that are quasi-equilibrated can be used to reduce the complexity of the reaction mechanism. Thus, an approach, preferably analytical, that identifies the key elementary reactions and surface intermediates is highly desirable. Additionally, if the rate-determining steps are identified then detailed quantum chemical calculations are required for only those reactions, while more approximate methods can be used for the remaining reactions. Recently, an analytical method was proposed using the maximum rates of the constituent steps to obtain the steady state kinetics of a reaction mechanism.<sup>43</sup>

In this analysis, the maximum rate of each elementary step is calculated by assuming that the transition state of each

elementary reaction is formed from the gas phase reactant and product in a lumped reaction and the lumped reaction is quasi-equilibrated. The degree of rate control of each elementary reaction is calculated from the maximum rate of constituent steps and the overall reaction rate is calculated using the degree of rate control and the maximum rate of an elementary step.

The maximum rate is calculated by assuming that the transition state is in equilibrium with the gas phase reactant. For example, the maximum rate of step 3,  $r_{\max,3}$ , in Figure 10 is:

$$r_{\max,3} = \frac{k_B T}{h} K_{eq,R \rightarrow TS_3} P_R \quad (35)$$

where  $K_{eq,R \rightarrow TS_3}$  is the equilibrium constant for the formation of the transition state of step 3 directly from the gas phase reactant. The change in Gibbs free energy for the formation of  $TS_3$  from  $R$  is equal to (see Figure 10):

$$\Delta G_{R \rightarrow TS_3}^g = \Delta G_{I_1}^o + \Delta G_{I_2}^o + E_{act,3} \quad (36)$$

where  $E_{act,3}$  is the activation energy of step 3. Thus, the equilibrium constant in eq 35 can be written as:

$$K_{eq,R \rightarrow TS_3} = K_{eq,1} K_{eq,2} K_{eq,3}^{\ddagger} \quad (37)$$

The maximum rate in eq 35 becomes:

$$r_{\max,3} = K_{eq,1} K_{eq,2} k_3 P_R \quad (38)$$

Similarly, the maximum rate of all elementary reactions can be calculated. The degree of rate control of each elementary step can be determined as:

$$X_{RC,i} = \frac{\frac{1}{r_{\max,i}}}{\sum_{k=1}^n \left( \frac{1}{r_{\max,k}} \right)} \quad (39)$$

The reaction steps with high degree of rate control are kinetically significant steps and more precise value of the activation energy for these steps must be calculated. In contrast, the activation energies of all the remaining steps are kinetically insignificant. Finally, the overall rate of the reaction can be estimated as:

$$r_{\text{overall}} = r_{\max,i} X_{\text{RC},i} (1 - \beta) \quad (40)$$

Here,  $\beta$  is the reversibility of the overall reaction.

It should be noted that in the above analysis the surface sites are not included, and thus, the results shown above are valid for catalytic reaction in the limit of low coverage of the catalytic sites. Accordingly, the results above are exact for the case where the fraction of free surface sites is unity and becomes approximate with increasing surface coverage by surface intermediates.

To account for the surface coverage by adsorbed intermediates, the value of the fraction of the free surface is required. The overall rate of the reaction, as a first approximation, can be estimated as:

$$r_{\text{overall}} = r_{\max,i} X_{\text{RC},i} (1 - \beta) \theta_*^n \quad (41)$$

where  $\theta_*$  is the fraction of free surface sites, and  $n$  is the number of surface sites involved in the  $i$ th elementary step. Next, we evaluate the limits on the fraction of free surface. For the reaction mechanism shown in Figure 10, the reversibility of each elementary step as well as the reversibility of the overall reaction is between 1 and 0, that is,

$$0 \leq \beta \leq 1 \text{ and } 0 \leq z_i \leq 1 \quad (42)$$

From eq 19, the overall reversibility of the reaction is:

$$\beta = z_1 z_2 z_3 z_4 \quad (43)$$

From eqs 42 and 43, we can write:

$$\beta \leq z_i \leq 1 \quad (44)$$

Using eqs 18 and 44, we get:

$$\begin{aligned} \beta &\leq \frac{\gamma_1}{K_1 P_R} \leq 1; \quad \beta \leq \frac{\gamma_2}{K_2 \gamma_1} \leq 1 \\ \beta &\leq \frac{\gamma_3}{K_3 \gamma_2} \leq 1; \quad \beta \leq \frac{P_p}{K_4 \gamma_3} \leq 1 \end{aligned} \quad (45)$$

where  $\gamma_i = \theta_{I_i}/\theta_*$ . The bounds on the surface coverages become:

$$\begin{aligned} \beta K_1 P_R &\leq \gamma_1 \leq K_1 P_R; \\ \beta K_2 K_1 P_R &\leq \gamma_2 \leq K_2 K_1 P_R; \\ \beta K_3 K_2 K_1 P_R &\leq \gamma_3 \leq K_3 K_2 K_1 P_R \end{aligned} \quad (46)$$

Applying the conservation of sites, we get:

$$\sum_i \theta_i = \theta_* (1 + \gamma_1 + \gamma_2 + \gamma_3) = 1 \quad (47)$$

$$\theta_* = \frac{1}{(1 + \gamma_1 + \gamma_2 + \gamma_3)} \quad (48)$$

Using eqs 46 and 48, we can determine the maximum and minimum value for the fraction of free surface sites as:

$$\begin{aligned} \theta_*^{\min} &= \frac{1}{(1 + \gamma_1^{\max} + \gamma_2^{\max} + \gamma_3^{\max})} \\ &= \frac{1}{(1 + K_1 P_R + K_1 K_2 P_R + K_1 K_2 K_3 P_R)} \\ \theta_*^{\max} &= \frac{1}{(1 + \gamma_1^{\min} + \gamma_2^{\min} + \gamma_3^{\min})} \\ &= \frac{1}{(1 + \beta K_1 P_R + \beta K_1 K_2 P_R + \beta K_1 K_2 K_3 P_R)} \end{aligned} \quad (49)$$

It should be noted that the maximum value of  $\theta_*$  is obtained when the approach to equilibrium is included in the analysis, and the minimum value of  $\theta_*$  is equivalent to the case where all species are quasi-equilibrated with the gas phase or the overall reaction is equilibrated.  $\theta_*^{\min}$  was used in ref 43, as a first approximation, to estimate the fraction of free surface sites. Application of  $\theta_*^{\min}$  in eq 41 gives the lower bound on the overall reaction rate. Alternatively, the maximum value of  $\theta_*$  (eq 49) can be used to determine the rate of the overall reaction. The maximum value of  $\theta_*$  is equivalent to the case where the overall reaction reversibility is equal to  $\beta$ . It should be noted that the surface coverages of reaction intermediate and thereby the reaction rate obtained from the above analysis will differ from the complete microkinetic analysis. We emphasize here that the maximum rate analysis is exact when the surface is clean and becomes approximate with increasing surface coverage.

The value of maximum rate analysis is to provide guidance to identify the important rate limiting reactions and potential abundant species that determine the performance of the catalyst. It is then possible to obtain precise values for the energies of a smaller subset of reaction intermediates and transition states that are kinetically significant for a more complete microkinetic analysis. In contrast, the binding energies of the remaining species are kinetically insignificant. It is important to note that the above analysis for surface coverage is accurate only for a catalytic reaction where there is one product and only one reaction route for a given intermediate. For intermediates that can be formed from multiple pathways, it is instructive to obtain the surface coverage from the pathway, which yields maximum surface coverage of the intermediate.

Additionally, the maximum rate analysis can be used to determine if a particular elementary step should be included in a reaction mechanism by a simple analysis: the maximum rates of all elementary steps should be greater than the experimentally measured rate of the overall reaction ( $r_{\text{exp}}$ ), that is,

$$r_{\max,i} \geq r_{\text{exp}} \quad (50)$$

For cases where eq 50 is not satisfied, those elementary reactions must not be included in the reaction mechanism.<sup>43</sup>

Maximum rate analysis was used to predict the turnover rate for the water gas shift reaction on a Cu catalyst.<sup>43</sup> Both redox and carboxyl pathways were studied using microkinetic modeling and maximum rate analysis. The reaction rate, activation energy, and reaction order predicted from maximum rate analysis were found to be in good agreement with the predictions from the microkinetic model and the experimental data. Figure 11 shows that the degree of rate control switches from CO<sub>2</sub> formation to water dissociation as the activation energy of water dissociation increases. Both the microkinetic model and maximum rate analysis correctly predict the change in degree of rate control from one elementary step to another.

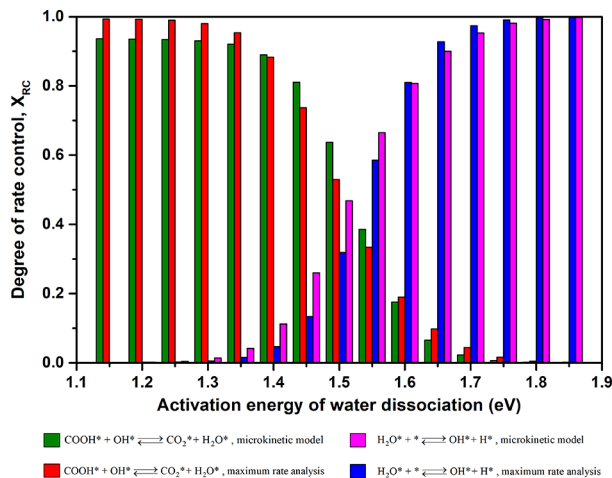


**Figure 11.** Comparison of the predicted degrees of rate control using a microkinetic model and maximum rate analysis for the water gas shift reaction. Reprinted with permission from ref 43. Copyright 2016 National Academy of Sciences.

## 7. RATE EXPRESSION ANALYSIS

Maximum rate analysis is a useful tool in analysis of reaction schemes, determining kinetically important reactions and intermediates and in prediction of the overall rate of the reaction. However, it requires data for the energies of all transition states and all adsorbed intermediates, and as such is not practical for reactions involving large molecules (due to prohibitive computational cost). A method to analyze reaction mechanism using generalized kinetic rate expressions was recently proposed.<sup>170</sup> This method is well suited for designing better catalyst where computational data are scarce but experimental data are available. In rate expression analysis, the rate expression, based on a conceived reaction mechanism and assumed rate-determining reactions, is written in terms of the transition states and adsorbed intermediates, such that the reaction order and apparent activation energy are in agreement with experimental data. The proposed rate expression along with scaling relations are used to design catalysts with improved performance.

An algorithm for obtaining a generalized rate expression is shown in Figure 12, wherein the rate is written as a function of the change in the binding energies of the transition state and most abundant surface intermediate (MASI) from a reference surface.

A generalized rate expression for a given rate mechanism is obtained by assuming certain rate-determining reactions and a most abundant surface intermediate. On the basis of these choices the reaction orders and activation energies are calculated and compared with the experimentally observed reaction orders and activation energy. The obtained rate expression can then be used to determine the optimal properties using scaling relations.

For a reaction mechanism with a single rate-determining step and a single MASI, the generalized rate expression was derived to be:<sup>170</sup>

$$r = \frac{r_{\max, \text{RDS}}^0 \exp\left(-\frac{\Delta BE_{\text{TS,RDS}}}{RT}\right)}{\left(1 + K_{\text{ads}, \text{MASI}}^0 \prod_k P_k^{-\nu_{k, \text{MASI}}} \exp\left(-\frac{\Delta BE_{\text{MASI}}}{RT}\right)\right)^n} \quad (51)$$

where  $r_{\max, \text{RDS}}^0$  is the maximum rate of the rate-determining step on the reference catalyst,  $\Delta BE_{\text{TS,RDS}}$  is the change in the binding

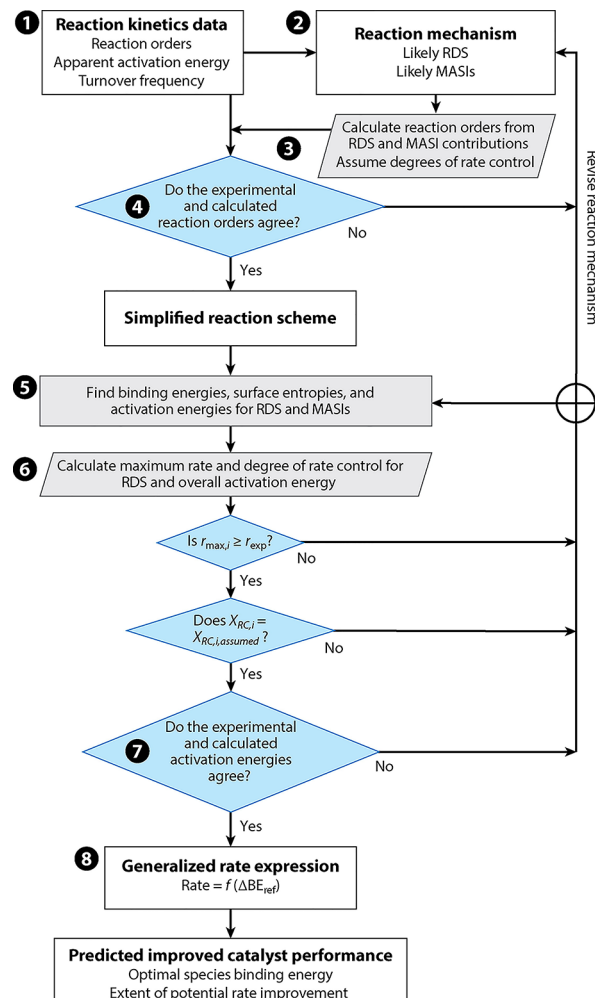


**Figure 12.** Algorithm for generating generalized two-step reaction kinetics rate expressions. The algorithm can be used to guide the search for improved catalyst performance in terms of binding energies for transition states and adsorbed species. Reprinted with permission from ref 170. Copyright 2018 Annual Reviews.

energy of the transition state of the rate-determining step from the reference surface,  $K_{\text{ads}, \text{MASI}}^0$  is the equilibrium constant for the formation of MASI on the reference catalyst, and  $\Delta BE_{\text{MASI}}$  is the change in the binding energy of the most abundant surface intermediate from the reference surface.

Using the scaling relationship between the binding energy of transition state of the rate-determining step and the binding energy of a descriptor, the change in the binding energy of the transition state and the descriptor can be written as:

$$\Delta BE_{\text{TS}} = \chi_{\text{TS}} \Delta BE_{\text{ref}} \quad (52)$$

where  $\Delta BE_{\text{ref}}$  is the change in the binding energy of the descriptor from the reference surface, and  $\chi_{\text{TS}}$  is the slope in the linear relationship between the transition state and the descriptor.

Similarly, the change in the binding energy of the MASI can be written as the function of change in the binding energy of the descriptor:

$$\Delta BE_{\text{MASI}} = \chi_{\text{MASI}} \Delta BE_{\text{ref}} \quad (53)$$

Using eqs 52 and 53, the generalized rate expression (eq 51) can be written as a function of a single variable,  $\Delta BE_{\text{ref}}$

$$r = \frac{r_{\max, \text{RDS}}^{\circ} \exp\left(-\frac{\chi_{\text{TS}} \Delta BE_{\text{ref}}}{RT}\right)}{\left(1 + K_{\text{ads}, \text{MASI}}^{\circ} \prod_k P_k^{-\nu_{k, \text{MASI}}} \exp\left(-\frac{\chi_{\text{MASI}} \Delta BE_{\text{ref}}}{RT}\right)\right)^n} \quad (54)$$

Eq 54 can be used to obtain the maximum rate that can be achieved by varying the kinetically significant parameters.

To demonstrate the capability of the rate expression analysis, ammonia synthesis was used as an example.<sup>170</sup> Iron (Fe) is the catalyst of choice for ammonia synthesis due to economic reasons and was used as the reference surface. The binding energy of nitrogen atom was used as a descriptor. Figure 13

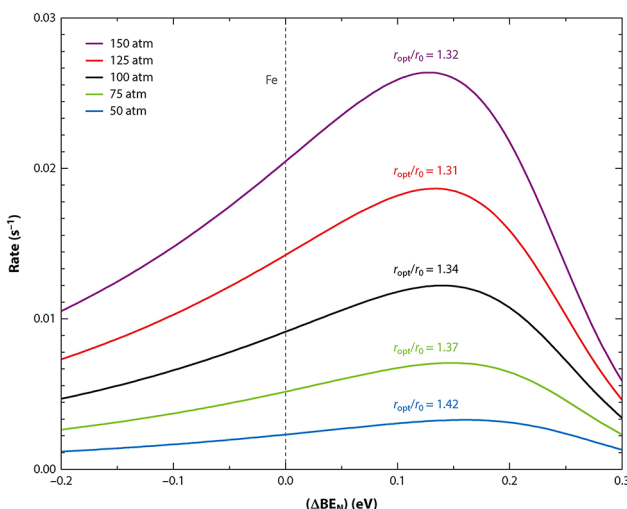


**Figure 13.** Turnover frequency of ammonia synthesis as a function of the change in nitrogen binding energy. Effect of total reaction pressure on reaction rate and potential rate enhancement,  $r_{\text{opt}}/r_0$  is shown. The binding energy of N on Fe is indicated by the dashed line. Reprinted with permission from ref 170. Copyright 2018 Annual Reviews.

shows the predicted rate at various reaction pressure using rate expression analysis.<sup>170</sup> With increasing pressure, the reaction rate increases, however the extent of potential rate improvement decreases. It is observed that the optimal catalyst should bind nitrogen weaker than Fe by 0.16 eV. This prediction is in agreement with previous work wherein it was demonstrated that the optimal catalyst for ammonia synthesis binds atomic nitrogen stronger than ruthenium but weaker than iron.<sup>83,209,244</sup> It should be noted that in this example the rate-determining step and the most abundant surface intermediate was assumed to remain same as the binding energy of the descriptor was varied. However, this approach is accurate only for the metals that are similar to the reference metal as the rate controlling step as well as the most abundant surface intermediate can change for a metal that is dissimilar to the reference metal. Thus, caution is warranted when using eqs 51 and 54, especially for cases where the binding energy of the descriptor is changed significantly from the reference surface.

For a reaction with multiple rate-determining steps, we refer the reader to the analysis presented in ref 170.

## 8. MICROKINETIC MODELS IN HOMOGENEOUS CATALYSIS

The use of microkinetic models has so far been rather scarce in computational homogeneous catalysis. The prominent reaction steps in a catalytic cycle can be often identified from

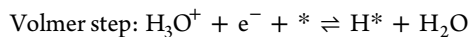
experimental data, however, there are well-documented examples wherein key short-lived intermediates were identified using computational methods.<sup>245–247</sup> The most practical interpretations have been conducted by the direct analysis of the potential energy surface to determine the most favorable reaction pathway based on the activation energy of the elementary steps.<sup>248–252</sup> In these cases, microkinetic modeling can be used to understand intricacies of a complicated reaction mechanism. Microkinetic modeling is an indispensable tool in studying large reaction mechanisms where the conventional analysis becomes difficult due to the size of the reaction network. Similarly, microkinetic modeling is useful in understanding reaction mechanism where intermediates are shared within multiple catalytic cycles. In these cases, the topology of the reaction mechanism makes it difficult to analyze potential energy surface for identification of viable reaction pathways and rate-determining reactions.

Additionally, microkinetic modeling can provide insight in cases where the relative concentrations of reactive intermediates differ by orders of magnitude. In these cases, analyzing just the potential energy surface may lead to erroneous conclusion as coverage effects of reactants, products and intermediates are ignored. The relative rates of elementary steps can be influenced not only by the activation energy of each elementary step but also by the concentrations of the intermediates that are reactants and products of those elementary steps. Extremely low concentrations of reactants/intermediates are present in many reaction systems including photocatalytic reactions, acid–base chemistry, and multiphase reactions wherein the concentrations of gases are limited by their solubility in the reaction medium. Conversely, there are cases where the concentration of a reactant may be high, especially for the case where solvent participates as a reactant in the system. For example, Maseras et al., studied the side reaction occurring during the activation of C–H bonds by metallocarbene complexes.<sup>253</sup> In this reaction, a diazo molecule reacts with a metal complex leading to the formation of catalytically active metallocarbene complex which reacts with an alkane molecule to activate the C–H bond. In the side reaction, the metallocarbene complex reacts with a diazo molecule to produce either fumarate or maleate. The energetics, calculated from DFT, are such that the activation barrier for dimerization is lower than that for alkane activation. An analysis solely based on free energy diagram leads to an erroneous conclusion that dimerization is favored over alkane activation, whereas high selectivity toward alkane functionalization is achieved under experimental condition. The key missing part is the relative concentration of the diazo molecule and alkane. Alkane being the solvent is present in high concentration whereas diazo molecule being a promotor is present in catalytic quantities and as such the rate of dimerization is much lower than that of C–H activation. Microkinetic modeling considers both the activation energy of each elementary step as well as the concentration of intermediates leading to a result that agrees with the experimental observations.

A microkinetic model can be used to determine the reaction flux and product selectivity as a function of reaction conditions, thereby providing invaluable insights regarding the reaction mechanism such that research effort can be efficiently focused on designing catalytic materials with improved performance.

## 9. MICROKINETIC MODELS IN ELECTROCATALYTIC APPLICATION

The need for advanced electro-catalysts for energy efficient and environmentally benign electrochemical conversion has grown notably in the past few decades.<sup>254–260</sup> Determining the rate controlling reactions and the effect of intermediate surface coverage on the overall reaction rate is critical in designing efficient electro-catalysts. In the classical analysis, experimentally observed Tafel slopes are compared with the theoretically derived slopes assuming different rate-determining elementary reactions and certain surface coverage.<sup>261–264</sup> Microkinetic models can assist in enhancing the mechanistic understanding of the reaction, thereby providing valuable information for rational catalyst design. Microkinetic modeling with DFT derived parameters have been used to predict catalytic activity for various electro-catalytic reactions.<sup>264–268</sup> Here, we discuss microkinetic modeling of hydrogen evolution reaction (HER). HER can proceed via hydronium ion reduction or water reduction. We will consider a simplified case where hydronium ion is reduced in a Volmer-Tafel mechanism:



The rate of the elementary reactions can be written as:

$$r_V = k_V a_{\text{H}_3\text{O}^+} \theta_* - k_{-V} \theta_{\text{H}} a_{\text{H}_2\text{O}} \quad (55)$$

$$r_T = k_T \theta_{\text{H}}^2 - k_{-T} \theta_*^2 a_{\text{H}_2} \quad (56)$$

where  $r_V$  and  $r_T$  are the rates of the Volmer and Tafel steps, respectively.  $k_V$  and  $k_{-V}$  are the forward and reverse rate constant for the Volmer step, respectively, and  $k_T$  and  $k_{-T}$  are the forward and reverse rate constant for the Tafel step, respectively. Because these steps are electron transfer steps, the rate constant depends on the applied potential:

$$k_i = k_i^o \exp\left[\frac{-\beta_i F}{RT}\eta\right] \quad (57)$$

$$k_{-i} = k_{-i}^o \exp\left[\frac{(1-\beta_i)F}{RT}\eta\right] \quad (58)$$

where,  $\eta$  is the overpotential.  $k_i^o$  and  $k_{-i}^o$  are the standard forward and reverse rate constant for  $i$ th elementary reaction at equilibrium ( $\eta = 0$ ), respectively.  $\beta_i$  is the symmetry factor for the  $i$ th elementary reaction. We reiterate here that the rate constants are not independent variables and must be thermodynamically consistent (i.e., the rate constants must satisfy eq 7 and eq 14).

For the Volmer-Tafel mechanism, at steady state, eq 4 becomes:

$$r_{\text{overall}} = \frac{r_V}{2} = \frac{r_T}{1} \quad (59)$$

since  $\sigma_V$  and  $\sigma_T$  are 2 and 1, respectively. Eq 59 along with the site balance can be solved to obtain the surface coverage and the overall rate of the reaction at specified reaction conditions. The electric current density is obtained from the reaction rate as:

$$i = nFr_{\text{overall}} \quad (60)$$

where  $i$  is the electric current density, and  $n$  is the number of electrons involved in the reaction. The current density can be

used to obtain the Tafel slope and the exchange current density,  $i_0$ , for any reaction condition. It should be noted that no assumptions regarding the rate-determining steps were made in the analysis, and this analysis is fundamentally different than the classical analysis wherein a rate-determining step and surface coverage is assumed. We note here that we used a simple case to demonstrate the microkinetic framework, however, a complicated reaction network can be easily analyzed with the same principles outlined above. Additionally, the effects of mass transport<sup>266</sup> adsorbate–adsorbate interaction (Temkin-like adsorption),<sup>268</sup> site blocking by spectator species,<sup>267</sup> anion effect, and local pH<sup>269–271</sup> can be easily incorporated. Furthermore, similar analysis to the one outlined for HER, can be applied to the oxygen evolution reaction (OER), oxygen reduction reaction (ORR), and hydrogen oxidation reaction (HOR). For a further detailed discussion on these reactions, we direct the reader to a recent report by Takanabe et al.<sup>272</sup>

We have shown that microkinetic modeling can be used to gain mechanistic understanding into electrochemical processes without preconceived assumptions regarding the nature of rate controlling steps and abundant surface intermediates. However, as noted in section 2.1, a detailed reaction mechanism is the first step in developing a microkinetic model and the complexity of some electrochemical reactions can be sufficiently high such that proposing a conclusive reaction mechanism may become challenging. For example, generating a complete reaction mechanism for CO<sub>2</sub> electroreduction to fuels is difficult as 16 different products including aldehydes, carboxylic acids and alcohols can be formed over the course of the reaction.<sup>273</sup> Additionally, it had been shown that the reaction flux through different reaction pathways leading to different products can vary significantly with catalyst structure<sup>274</sup> as well as operating conditions like pH and composition of the electrolyte.<sup>275</sup> Even with these challenges, our understanding of the electrochemical systems has improved significantly in the past two decades, owing to well-designed experiments along with carefully conducted theoretical work.<sup>276</sup> Moving forward, we foresee that improved understanding of the reaction mechanism will be obtained through operando characterization techniques like surface enhanced infrared adsorption spectroscopy,<sup>277,278</sup> surface-enhanced Raman spectroscopy,<sup>279</sup> in situ X-ray absorption spectroscopy,<sup>65</sup> together with improved DFT studies using accurate exchange-correlation functionals that correctly describe electrolyte effects,<sup>280</sup> molecule solvation, surface–adsorbate interactions and electric double layer,<sup>281</sup> and combined with well-designed isotopic labeling experiments.<sup>282</sup> We envision that with the improvement in our understanding of reaction mechanisms, microkinetic modeling will play a crucial role in identifying the relative importance of various effects and will guide in rational catalyst as well as process design.

## 10. MICROKINETIC MODELING OF TRANSIENT KINETICS

Steady state experiments are the most common type of experiments performed in a laboratory due to the simplicity of operations and simple analysis of data. The steady state reaction kinetics provide information about the activity, selectivity, reaction orders and apparent activation energy of the reaction over a catalyst. Transient analysis techniques are powerful tools for gaining insight in the reaction mechanism of complex reactions and have been used to obtain critical information for many industrially relevant reactions. Transient analysis techniques provide an opportunity to directly measure the

surface coverage and lifetime of reaction intermediates, thus providing critical information about reaction chemistry, including identification of the most abundant surface intermediate, reaction sequence in a multistep reaction mechanism and the rate constant of elementary steps.<sup>283–291</sup> However, the analysis of transient experiments is challenging, and the difficulty in data analysis is increased when more than one rate-determining steps are present.<sup>292</sup> In these cases, microkinetic modeling can be used to understand the transient response and obtain valuable information regarding the reaction mechanism. Recently, various studies have used microkinetic modeling to complement experimental transient studies.<sup>166,292–296</sup> As an example, Hensen et al. used microkinetic modeling to obtain significant insights into the surface kinetics of CO hydrogenation over Co catalysts.<sup>292</sup> They found that CO scission on an empty surface is initially fast after which the overall rate is limited by carbon hydrogenation and that the surface coverage of hydrogen affects CO desorption leading to increased CO retention on the catalyst surface and higher methanation rates. Furthermore, the microkinetic model can be used to determine the transient response of the degree of rate control.<sup>194</sup> Next, we briefly describe the development of microkinetic model for transient analysis.

Transient experiments are typically carried out in a flow microreactor due to the low reactor volume and operational simplicity. Additionally, the reactors are operated with short residence time of reactants leading to differential conversion. Consequently, the differential bed micro-PFR can be modeled as a transient CSTR. The material balance for a species  $i$  in a transient CSTR operating at constant total pressure for an ideal gas mixture can be written as:

$$\frac{dF_i}{dt} = F_i^{\circ} - F_i + \Omega_i \quad (61)$$

where  $F_i$  and  $F_i^{\circ}$  are the inlet and outlet flow rate of species  $i$  normalized by the total number of surface sites in the reactor, respectively, and  $\Omega_i$  is the turnover frequency for the production of species  $i$ . Eq 61 is valid under differential conditions as the change in the total number of moles, and the total heat generated upon reaction is negligible. The rate of change of coverage of the adsorbed species is described by:

$$\frac{\partial \theta_j}{\partial t} = \sum_i \nu_{ij} r_i \quad (62)$$

where  $r_i$  is the rate of each elementary reaction as defined in eq 15, and  $\nu_{ij}$  is the stoichiometric coefficient of species  $j$  in the elementary step  $i$ . Eqs 61 and 62 are solved numerically along with the site balance to obtain the overall reaction rate as well as the transient coverage of all species.

## CONCLUDING REMARKS AND OUTLOOK

This review has addressed the development and analysis of microkinetic models for systematic elucidation of reaction mechanisms. Using recent examples from the literature, it was shown that microkinetic modeling provides essential insights for the development of catalysts with improved performance. In macro-kinetic modeling, a rate expression is obtained by making assumptions about rate-determining reactions and abundant surface intermediates, and rate constants, reaction orders, and activation energies are obtained using regression of experimental data. In microkinetic modeling, rate constants are estimated using first principle calculations and no assumptions about the

rate-determining reactions or most abundant surface species are made. Rather the information regarding the rate-determining reactions, concentrations or surface coverages of the reaction intermediates, reaction orders, and apparent activation energy is obtained as a result of the analysis of the microkinetic models. The information obtained from microkinetic analysis allows the researcher to identify material properties for enhanced catalytic performance.

Here, we outlined the framework required to perform microkinetic modeling. Throughout this review, we outline the assumptions that are made to obtain the required parameters to construct a microkinetic model. We discuss the consequences of these assumptions and scenarios where making certain assumptions leads to erroneous conclusions. We discuss various techniques, like sensitivity analysis and the degree of rate control, for analyzing and obtaining critical information from the microkinetic models. Using examples from the literature, we show that these tools are useful in drawing meaningful conclusions from the model. We discuss the incorporation of Brønsted–Evans–Polanyi and scaling relations in microkinetic models and the effect of these correlation on catalytic performance and formation of volcano curves. These relationships impose fundamental constraints on the extent of potential rate enhancement that can be achieved. Microkinetic modeling provides a framework that helps the researcher in identifying the bottlenecks for designing materials that may break these scaling relations to outperform traditional catalysts. Significant improvements in kinetic parameter estimation have been made, and with these improvements the assumptions made in performing microkinetic modeling are relaxed. Studies that include surface coverage effects, multiple active sites, surface ligand effects, and metal nanostructures have improved our understanding of various reaction mechanisms and helped in developing more efficient catalysts.

Microkinetic modeling requires the thermodynamic properties of all adsorbed species and rate constants for all elementary surface reactions; however, the overall reaction rate is controlled by only a few key parameters, that is, the activation energies of the rate-determining reactions and adsorption energies of most abundant surface intermediates. Thus, it is desirable to identify these species such that detailed calculations using electronic structure calculations can be carried out for these species and approximate methods can be used for all other species, thereby reducing the overall computational cost. Maximum rate analysis can be used to identify transition states and adsorbed species that are kinetically important in controlling catalyst performance. Additionally, maximum rate analysis can be used to simplify the reaction mechanism by eliminating reaction pathways where the maximum rate is lower than the experimentally observed reaction rates.

The above-discussed modeling approaches are useful for cases where the kinetic parameters are either available or can be estimated using quantum chemical calculations. For the cases where the kinetic parameters are not easily available, an approach that combines maximum rate analysis and experimental data can be used. A general reaction kinetics rate expression can be written in terms of reference binding energies, which allows for the prediction of the extent of potential rate improvement, optimal surface coverage, and optimal binding energies of adsorbed species.

Finally, we discuss the application of microkinetic modeling in homogeneous catalysis, electro-catalysis, and transient reaction kinetics. Applications of microkinetic modeling in these areas

are now emerging, and we anticipate that the success of microkinetic modeling in elucidation of reaction mechanisms and identification of improved catalytic materials in heterogeneous catalysis will inspire confidence in researchers in related fields to adopt these methodologies in guiding their search for improved catalysts.

## APPENDIX I

The standard enthalpy change,  $\Delta H_i^o$ , for an elementary step is:

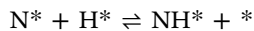
$$\Delta H_i^o = \sum_{\text{products}} H_p^o - \sum_{\text{reactants}} H_r^o \quad (63)$$

Eq 63 can be written in terms of enthalpy change in the gas phase and the change in the binding energies as:

$$\Delta H_i^o = \Delta H_{i,\text{gas}}^o + \Delta BE_i \quad (64)$$

An advantage of using eq 64 is that thermodynamic consistency is always maintained (see section 2.4).

For example, consider the following elementary reaction occurring during ammonia synthesis (Step 3 in Table 3),



The enthalpy change in the gas phase for this elementary reaction is:

$$\Delta H_{i,\text{gas}}^o = H_{\text{NH},\text{gas}}^o - H_{\text{H},\text{gas}}^o - H_{\text{N},\text{gas}}^o \quad (65)$$

The gas phase enthalpies can be readily obtained from standard tables for many species. For instance, when the gas phase enthalpies are not available from the literature, the gas phase enthalpies can be calculated using quantum chemical methods. The change in the binding energy is:

$$\Delta BE = BE_{\text{NH}} - BE_{\text{H}} - BE_{\text{N}} \quad (66)$$

As discussed in section 2.3, the binding energies of intermediates can be obtained from experimental data or can be estimated by quantum chemical calculations.

The standard entropy change,  $\Delta S_i^o$ , for an elementary step is:

$$\Delta S_i^o = \sum_{\text{products}} S_p^o - \sum_{\text{reactants}} S_r^o \quad (67)$$

The standard entropy of intermediates can be obtained from experimental data or can be estimated by quantum chemical calculations. The entropy change of a surface reaction is small compared to the enthalpy change of a gas phase reaction, and as such, entropic contributions to the rate constant and equilibrium constant are relatively small. However, the entropy changes for adsorption and desorption steps are large as the adsorbing/desorbing molecule loses/gains translational entropy. Additionally, the entropic contributions to the rate constant and equilibrium constant are significant for reactions operating at high temperature and must be carefully evaluated.<sup>297</sup> For the cases where entropy of a species is not available, statistical thermodynamic is used to estimate the entropy:

$$S_i^o = S_{i,\text{translational}}^o + S_{i,\text{rotational}}^o + S_{i,\text{vibrational}}^o \quad (68)$$

where the entropy of a species is the sum of the contributions from translational, rotational, and vibrational modes of motion. In general, the electronic and nuclear contributions to the entropy of a molecule are small and are generally neglected. The expression for standard translational entropy of a molecule is:

$$S_{\text{translational}}^o = R \left[ \ln \left( \frac{(2\pi m k_B T)^{3/2} k_B T}{h^2} \right) + \frac{5}{2} \right] \quad (69)$$

where  $P^\circ$  is the standard state pressure. The expression for the rotational entropy of a nonlinear molecule is:

$$S_{\text{rotational}}^o = R \left[ \ln \left( \frac{8\pi^2 \sqrt{8\pi^3 I_x I_y I_z}}{\sigma_r} \left( \frac{k_B T}{h^2} \right)^{3/2} \right) + \frac{3}{2} \right] \quad (70)$$

where  $I_x$ ,  $I_y$ , and  $I_z$  are the moment of inertia around the principle axis of rotation, and  $\sigma_r$  is the rotation symmetry number. For a linear molecule, the expression for rotational entropy reduces to:

$$S_{\text{rotational}}^o = R \left[ \ln \left( \frac{8\pi^2 I_{\text{linear}}}{\sigma_r} \left( \frac{k_B T}{h^2} \right) \right) + 1 \right] \quad (71)$$

where  $I_{\text{linear}}$  is the moment of inertia of the molecule about the molecular axis. The expression for the vibrational entropy of the gas phase molecule is:

$$S_{\text{vibrational}}^o = R \sum_j^{\text{modes}} \left( \frac{h\nu_j}{k_B T(e^{(h\nu_j/k_B T)} - 1)} - \ln(1 - e^{-(h\nu_j/k_B T)}) \right) \quad (72)$$

where  $\nu_j$  is the frequency of the  $j$ th vibrational mode.

For adsorbed species and transition states, the translational and rotational modes are replaced by frustrated vibrational modes. Thus, the vibrational entropy is estimated using eq 72. The vibrational frequencies of the adsorbed species are obtained from the literature using vibrational spectra or from quantum chemical calculations.

The estimation of the standard entropy of an adsorbed molecule is discussed in detail by Campbell et al.<sup>42,298</sup>

## AUTHOR INFORMATION

### Corresponding Authors

**James A. Dumesic** — Department of Chemical and Biological Engineering, University of Wisconsin-Madison, Madison, Wisconsin 53706, United States;  [orcid.org/0000-0001-6542-0856](https://orcid.org/0000-0001-6542-0856); Email: [jdumesic@wisc.edu](mailto:jdumesic@wisc.edu)

**Ali Hussain Motagamwala** — Department of Chemical and Biological Engineering, University of Wisconsin-Madison, Madison, Wisconsin 53706, United States;  [orcid.org/0000-0002-9314-9028](https://orcid.org/0000-0002-9314-9028); Email: [motagamwala@wisc.edu](mailto:motagamwala@wisc.edu)

Complete contact information is available at:

<https://pubs.acs.org/10.1021/acs.chemrev.0c00394>

### Notes

The authors declare no competing financial interest.

### Biographies

Ali Hussain Motagamwala earned his B.Tech. (Hons.) degree in chemical engineering from Birla Institute of Technology and Science, India. He completed his master's degree in chemical engineering at the University of Toronto under the direction of Prof. Arun Ramachandran. He earned his Ph.D. degree under the supervision of Professor James Dumesic at the University of Wisconsin-Madison. During his Ph.D., he worked on microkinetic modeling, maximum rate analysis, and biomass upgrading to fuels and chemicals. After graduating from UW-Madison, he was a postdoctoral fellow with Professor Suljo Linic, investigating the dehydrogenation of light alkanes and oxidative coupling of

methane. In 2020, he joined the Shell Chemical Company as a research engineer.

Professor James A. Dumesic earned his B.S. degree from UW-Madison and his M.S. and Ph.D. degrees from Stanford University, under the supervision of Professor Michel Boudart. He joined the Department of Chemical Engineering at UW-Madison in 1976 and after a 43-year career in catalysis at UW-Madison, he retired in 2019. Throughout his career, he used the state-of-the-art spectroscopic, microcalorimetric, and reaction kinetics techniques to study the surface and dynamic properties of heterogeneous catalysts. He has authored over 570 articles in peer-reviewed scientific journals. Dumesic has received numerous research awards for his work on heterogeneous catalysis, the most recent being the 2019 ENI Energy Transition award that honors research and technological innovation that promotes the transition toward low-carbon energy systems. Dumesic pioneered the field of microkinetic analysis, in which diverse information from experimental and theoretical studies is combined to elucidate the essential surface chemistry that controls catalyst performance. He coauthored the highly cited book titled “The Microkinetics of Heterogeneous Catalysis”.

## ACKNOWLEDGMENTS

This material is based upon work supported by the US Department of Energy (DOE), Office of Science, Office of Basic Energy Sciences, Chemical Sciences, Geosciences, and Biosciences Division, under Contract No. DE-SC0014058.

## DEDICATION

This review is dedicated to the memory of Dr. Henrik Topsøe, who was a strong advocate for the use of microkinetic analysis (combined with *in situ* spectroscopic studies) in catalysis research.

## REFERENCES

- (1) Boudart, M. From the Century of the Rate Equation to the Century of the Rate Constants: A Revolution in Catalytic Kinetics and Assisted Catalyst Design. *Catal. Lett.* **2000**, *65*, 1–3.
- (2) Urmès, C.; Schweitzer, J.-M.; Cabiac, A.; Schuurman, Y. Kinetic Study of the Selective Hydrogenation of Acetylene over Supported Palladium under Tail-End Conditions. *Catalysts* **2019**, *9*, 180.
- (3) Molero, H.; Bartlett, B. F.; Tysoe, W. T. The Hydrogenation of Acetylene Catalyzed by Palladium: Hydrogen Pressure Dependence. *J. Catal.* **1999**, *181*, 49–56.
- (4) Bos, A. N. R.; Botsma, E. S.; Foeth, F.; Sleyster, H. W. J.; Westerterp, K. R. A Kinetic Study of the Hydrogenation of Ethyne and Ethene on a Commercial Pd/Al<sub>2</sub>O<sub>3</sub> Catalyst. *Chem. Eng. Process.* **1993**, *32*, 53–63.
- (5) Pachulski, A.; Schödel, R.; Claus, P. Kinetics and Reactor Modeling of a Pd-Ag/Al<sub>2</sub>O<sub>3</sub> Catalyst during Selective Hydrogenation of Ethyne. *Appl. Catal., A* **2012**, *445–446*, 107–120.
- (6) Borodziński, A.; Cybulski, A. The Kinetic Model of Hydrogenation of Acetylene-Ethylene Mixtures over Palladium Surface Covered by Carbonaceous Deposits. *Appl. Catal., A* **2000**, *198*, 51–66.
- (7) Jarullah, A. T.; Mujtaba, I. M.; Wood, A. S. Kinetic Model Development and Simulation of Simultaneous Hydrodenitrogenation and Hydrodemetallization of Crude Oil in Trickle Bed Reactor. *Fuel* **2011**, *90*, 2165–2181.
- (8) Tirado, A.; Ancheyta, J.; Trejo, F. Kinetic and Reactor Modeling of Catalytic Hydrotreatment of Vegetable Oils. *Energy Fuels* **2018**, *32*, 7245–7261.
- (9) Roininen, J.; Alopaeus, V.; Toppinen, S.; Aittamaa, J. Modeling and Simulation of an Industrial Trickle-Bed Reactor for Benzene Hydrogenation: Model Validation against Plant Data. *Ind. Eng. Chem. Res.* **2009**, *48*, 1866–1872.
- (10) Caputo, T.; Lisi, L.; Pirone, R.; Russo, G. Kinetics of the Preferential Oxidation of CO over CuO/CeO<sub>2</sub> Catalysts in H<sub>2</sub>-Rich Gases. *Ind. Eng. Chem. Res.* **2007**, *46*, 6793–6800.
- (11) Toppinen, S.; Rantakylä, T. K.; Salmi, T.; Aittamaa, J. Kinetics of the Liquid-Phase Hydrogenation of Benzene and Some Monosubstituted Alkylbenzenes over a Nickel Catalyst. *Ind. Eng. Chem. Res.* **1996**, *35*, 1824–1833.
- (12) Temkin, M. I. *Adv. Catal.*, 1st ed.; Eley, D. D., Pines, H., Weisz, P. B., Eds.; Academic Press: Burlington, 1979; Vol. 28.
- (13) Temkin, M. I.; Pyzhev, V. Kinetics of Ammonia Synthesis on Promoted Iron Catalysts. *Acta Physiochim.* **1940**, *12*, 217–221.
- (14) Emmett, P. H.; Kummer, J. T. Kinetics of Ammonia Synthesis. *Ind. Eng. Chem.* **1943**, *35*, 677–683.
- (15) Dumesic, J. A.; Rudd, D. A.; Aparicio, L. M.; Rekoske, J. E.; Trevino, A. A. *The Microkinetics of Heterogeneous Catalysis*, 1st ed.; American Chemical Society (ACS), 1993.
- (16) Carrasquillo-Flores, R.; Gallo, J. M. R.; Hahn, K.; Dumesic, J. A.; Mavrikakis, M. Density Functional Theory and Reaction Kinetics Studies of the Water-Gas Shift Reaction on Pt-Re Catalysts. *ChemCatChem* **2013**, *5*, 3690–3699.
- (17) Jacobsen, C. J. H.; Dahl, S.; Boisen, A.; Clausen, B. S.; Topsøe, H.; Logadottir, A.; Nørskov, J. K. Optimal Catalyst Curves: Connecting Density Functional Theory Calculations with Industrial Reactor Design and Catalyst Selection. *J. Catal.* **2002**, *205*, 382–387.
- (18) Gokhale, A. A.; Dumesic, J. A.; Mavrikakis, M. On the Mechanism of Low-Temperature Water Gas Shift Reaction on Copper. *J. Am. Chem. Soc.* **2008**, *130*, 1402–1414.
- (19) Plauck, A.; Stangland, E. E.; Dumesic, J. A.; Mavrikakis, M. Active Sites and Mechanisms for H<sub>2</sub>O<sub>2</sub> Decomposition over Pd Catalysts. *Proc. Natl. Acad. Sci. U. S. A.* **2016**, *113*, E1973–E1982.
- (20) Thybaut, J. W.; Sun, J.; Olivier, L.; Van Veen, A. C.; Mirodatos, C.; Marin, G. B. Catalyst Design Based on Microkinetic Models: Oxidative Coupling of Methane. *Catal. Today* **2011**, *159*, 29–36.
- (21) Stegelmann, C.; Stoltze, P. Microkinetic Analysis of Transient Ethylene Oxidation Experiments on Silver. *J. Catal.* **2004**, *226*, 129–137.
- (22) Yoo, J. S.; Abild-Pedersen, F.; Nørskov, J. K.; Studt, F. Theoretical Analysis of Transition-Metal Catalysts for Formic Acid Decomposition. *ACS Catal.* **2014**, *4*, 1226–1233.
- (23) Stoltze, P.; Nørskov, J. K. The Surface Science Based Ammonia Kinetics Revisited. *Top. Catal.* **1994**, *1*, 253–263.
- (24) Sun, J.; Thybaut, J. W.; Marin, G. B. Microkinetics of Methane Oxidative Coupling. *Catal. Today* **2008**, *137*, 90–102.
- (25) Grabow, L. C.; Mavrikakis, M. Mechanism of Methanol Synthesis on Cu through CO<sub>2</sub> and CO Hydrogenation. *ACS Catal.* **2011**, *1*, 365–384.
- (26) Sutton, J. E.; Panagiotopoulou, P.; Verykios, X. E.; Vlachos, D. G. Combined DFT, Microkinetic, and Experimental Study of Ethanol Steam Reforming on Pt. *J. Phys. Chem. C* **2013**, *117*, 4691–4706.
- (27) Christiansen, M. A.; Mpourmpakis, G.; Vlachos, D. G. DFT-Driven Multi-Site Microkinetic Modeling of Ethanol Conversion to Ethylene and Diethyl Ether on γ-Al<sub>2</sub>O<sub>3</sub>(111). *J. Catal.* **2015**, *323*, 121–131.
- (28) Greeley, J.; Mavrikakis, M. Competitive Paths for Methanol Decomposition on Pt(111). *J. Am. Chem. Soc.* **2004**, *126*, 3910–3919.
- (29) Kandoi, S.; Greeley, J.; Sanchez-Castillo, M. A.; Evans, S. T.; Gokhale, A. A.; Dumesic, J. A.; Mavrikakis, M. Prediction of Experimental Methanol Decomposition Rates on Platinum from First Principles. *Top. Catal.* **2006**, *37*, 17–27.
- (30) Kandoi, S.; Greeley, J.; Simonetti, D.; Shabaker, J.; Dumesic, J. A.; Mavrikakis, M. Reaction Kinetics of Ethylene Glycol Reforming over Platinum in the Vapor versus Aqueous Phases. *J. Phys. Chem. C* **2011**, *115*, 961–971.
- (31) Madon, R. J.; Braden, D.; Kandoi, S.; Nagel, P.; Mavrikakis, M.; Dumesic, J. A. Microkinetic Analysis and Mechanism of the Water Gas Shift Reaction over Copper Catalysts. *J. Catal.* **2011**, *281*, 1–11.
- (32) Singh, S.; Li, S.; Carrasquillo-Flores, R.; Alba-Rubio, A. C.; Dumesic, J. A.; Mavrikakis, M. Formic Acid Decomposition on Au

- Catalysts: DFT, Microkinetic Modeling, and Reaction Kinetics Experiments. *AIChE J.* **2014**, *60*, 1303–1319.
- (33) Alexopoulos, K.; John, M.; Van Der Borght, K.; Galvita, V.; Reyniers, M. F.; Marin, G. B. DFT-Based Microkinetic Modeling of Ethanol Dehydration in H-ZSM-5. *J. Catal.* **2016**, *339*, 173–185.
- (34) Aparicio, L. M.; Dumesic, J. A. Ammonia Synthesis Kinetics: Surface Chemistry, Rate Expressions, and Kinetic Analysis. *Top. Catal.* **1994**, *1*, 233–252.
- (35) Maestri, M.; Vlachos, D. G.; Beretta, A.; Groppi, G.; Tronconi, E. Steam and Dry Reforming of Methane on Rh: Microkinetic Analysis and Hierarchy of Kinetic Models. *J. Catal.* **2008**, *259*, 211–222.
- (36) Lozano-Blanco, G.; Thybaut, J. W.; Surla, K.; Galtier, P.; Marin, G. B. Fischer–Tropsch Synthesis: Development of a Microkinetic Model for Metal Catalysis. *Oil Gas Sci. Technol.* **2006**, *61*, 489–496.
- (37) Kandoi, S.; Gokhale, A. A.; Grabow, L. C.; Dumesic, J. A.; Mavrikakis, M. Why Au and Cu Are More Selective than Pt for Preferential Oxidation of CO at Low Temperature. *Catal. Lett.* **2004**, *93*, 93–100.
- (38) Jørgensen, M.; Grönbeck, H. First-Principles Microkinetic Modeling of Methane Oxidation over Pd(100) and Pd(111). *ACS Catal.* **2016**, *6*, 6730–6738.
- (39) Hansgen, D. A.; Vlachos, D. G.; Chen, J. G. Using First Principles to Predict Bimetallic Catalysts for the Ammonia Decomposition Reaction. *Nat. Chem.* **2010**, *2*, 484–489.
- (40) Salciccioli, M.; Vlachos, D. G. Kinetic Modeling of Pt Catalyzed and Computation-Driven Catalyst Discovery for Ethylene Glycol Decomposition. *ACS Catal.* **2011**, *1*, 1246–1256.
- (41) Schumacher, N.; Boisen, A.; Dahl, S.; Gokhale, A. A.; Kandoi, S.; Grabow, L. C.; Dumesic, J. A.; Mavrikakis, M.; Chorkendorff, I. Trends in Low-Temperature Water-Gas Shift Reactivity on Transition Metals. *J. Catal.* **2005**, *229*, 265–275.
- (42) Sprowl, L. H.; Campbell, C. T.; Árnadóttir, L. Hindered Translator and Hindered Rotor Models for Adsorbates: Partition Functions and Entropies. *J. Phys. Chem. C* **2016**, *120*, 9719–9731.
- (43) Motagamwala, A. H.; Dumesic, J. A. Analysis of Reaction Schemes Using Maximum Rates of Constituent Steps. *Proc. Natl. Acad. Sci. U. S. A.* **2016**, *113*, E2879–E2888.
- (44) Carrasquillo-Flores, R.; Ro, I.; Kumbhalkar, M. D.; Burt, S.; Carrero, C. A.; Alba-Rubio, A. C.; Miller, J. T.; Hermans, I.; Huber, G. W.; Dumesic, J. A. Reverse Water-Gas Shift on Interfacial Sites Formed by Deposition of Oxidized Molybdenum Moieties onto Gold Nanoparticles. *J. Am. Chem. Soc.* **2015**, *137*, 10317–10325.
- (45) Ulissi, Z. W.; Medford, A. J.; Bligaard, T.; Nørskov, J. K. To Address Surface Reaction Network Complexity Using Scaling Relations Machine Learning and DFT Calculations. *Nat. Commun.* **2017**, *8*, 1–7.
- (46) Inderwildi, O. R.; Jenkins, S. J.; King, D. A. Fischer–Tropsch Mechanism Revisited: Alternative Pathways for the Production of Higher Hydrocarbons from Synthesis Gas. *J. Phys. Chem. C* **2008**, *112*, 1305–1307.
- (47) Aguirre, A.; Collins, S. E. Selective Detection of Reaction Intermediates Using Concentration-Modulation Excitation DRIFT Spectroscopy. *Catal. Today* **2013**, *205*, 34–40.
- (48) Zhu, H.; Kwak, J. H.; Peden, C. H. F.; Szanyi, J. In Situ DRIFTS-MS Studies on the Oxidation of Adsorbed NH<sub>3</sub> by NO<sub>x</sub> over a Cu-SSZ-13 Zeolite. *Catal. Today* **2013**, *205*, 16–23.
- (49) Hibbitts, D.; Dybeck, E.; Lawlor, T.; Neurock, M.; Iglesia, E. Preferential Activation of CO near Hydrocarbon Chains during Fischer–Tropsch Synthesis on Ru. *J. Catal.* **2016**, *337*, 91–101.
- (50) Kumar, A.; Medhekar, V.; Harold, M. P.; Balakotaiah, V. NO Decomposition and Reduction on Pt/Al<sub>2</sub>O<sub>3</sub> Powder and Monolith Catalysts Using the TAP Reactor. *Appl. Catal., B* **2009**, *90*, 642–651.
- (51) Bai, Y.; Mavrikakis, M. Mechanistic Study of Nitric Oxide Reduction by Hydrogen on Pt(100) (I): A DFT Analysis of the Reaction Network. *J. Phys. Chem. B* **2018**, *122*, 432–443.
- (52) Scaranto, J.; Mavrikakis, M. Density Functional Theory Studies of HCOOH Decomposition on Pd(111). *Surf. Sci.* **2016**, *650*, 111–120.
- (53) Samjeské, G.; Miki, A.; Ye, S.; Osawa, M. Mechanistic Study of Electrocatalytic Oxidation of Formic Acid at Platinum in Acidic Solution by Time-Resolved Surface-Enhanced Infrared Absorption Spectroscopy. *J. Phys. Chem. B* **2006**, *110*, 16559–16566.
- (54) de Oliveira, L. P.; Hudebine, D.; Guillaume, D.; Verstraete, J. J. A Review of Kinetic Modeling Methodologies for Complex Processes. *Oil Gas Sci. Technol.* **2016**, *71*, 45.
- (55) Froment, G. F. Single Event Kinetic Modeling of Complex Catalytic Processes. *Catal. Rev.: Sci. Eng.* **2005**, *47*, 83–124.
- (56) Aghalayam, P.; Park, Y. K.; Vlachos, D. G. Construction and Optimization of Complex Surface-Reaction Mechanisms. *AIChE J.* **2000**, *46*, 2017–2029.
- (57) Fooshee, D.; Mood, A.; Gutman, E.; Tavakoli, M.; Urban, G.; Liu, F.; Huynh, N.; Van Vranken, D.; Baldi, P. Deep Learning for Chemical Reaction Prediction. *Mol. Syst. Des. Eng.* **2018**, *3*, 442–452.
- (58) Khan, S. S.; Zhang, Q.; Broadbelt, L. J. Automated Mechanism Generation. Part 1: Mechanism Development and Rate Constant Estimation for VOC Chemistry in the Atmosphere. *J. Atmos. Chem.* **2009**, *63*, 125–156.
- (59) Zhang, S.; Broadbelt, L. J.; Androulakis, I. P.; Ierapetritou, M. G. Reactive Flow Simulation Based on the Integration of Automated Mechanism Generation and On-the-Fly Reduction. *Energy Fuels* **2014**, *28*, 4801–4811.
- (60) Goldsmith, C. F.; West, R. H. Automatic Generation of Microkinetic Mechanisms for Heterogeneous Catalysis. *J. Phys. Chem. C* **2017**, *121*, 9970–9981.
- (61) Rangarajan, S.; Bhan, A.; Daoutidis, P. Identification and Analysis of Synthesis Routes in Complex Catalytic Reaction Networks for Biomass Upgrading. *Appl. Catal., B* **2014**, *145*, 149–160.
- (62) Rangarajan, S.; Kaminski, T.; Van Wyk, E.; Bhan, A.; Daoutidis, P. Language-Oriented Rule-Based Reaction Network Generation and Analysis: Algorithms of RING. *Comput. Chem. Eng.* **2014**, *64*, 124–137.
- (63) Rangarajan, S.; Brydon, R. R. O.; Bhan, A.; Daoutidis, P. Automated Identification of Energetically Feasible Mechanisms of Complex Reaction Networks in Heterogeneous Catalysis: Application to Glycerol Conversion on Transition Metals. *Green Chem.* **2014**, *16*, 813–823.
- (64) Sutton, J. E.; Vlachos, D. G. Building Large Microkinetic Models with First-Principles' Accuracy at Reduced Computational Cost. *Chem. Eng. Sci.* **2015**, *121*, 190–199.
- (65) Simm, G. N.; Vaucher, A. C.; Reiher, M. Exploration of Reaction Pathways and Chemical Transformation Networks. *J. Phys. Chem. A* **2019**, *123*, 385–399.
- (66) Broadbelt, L. J.; Stark, S. M.; Klein, M. T. Computer Generated Pyrolysis Modeling: On-the-Fly Generation of Species, Reactions, and Rates. *Ind. Eng. Chem. Res.* **1994**, *33*, 790–799.
- (67) Broadbelt, L. J.; Stark, S. M.; Klein, M. T. Termination of Computer-Generated Reaction Mechanisms: Species Rank-Based Convergence Criterion. *Ind. Eng. Chem. Res.* **1995**, *34*, 2566–2573.
- (68) Klinke, D. J.; Broadbelt, L. J. Mechanism Reduction during Computer Generation of Compact Reaction Models. *AIChE J.* **1997**, *43*, 1828–1837.
- (69) Broadbelt, L. J.; Stark, S. M.; Klein, M. T. Computer Generated Reaction Modelling: Decomposition and Encoding Algorithms for Determining Species Uniqueness. *Comput. Chem. Eng.* **1996**, *20*, 113–129.
- (70) Valdés-Perez, R. E.; Zeigarnik, A. V. Interactive Elucidation (without Programming) of Reaction Mechanisms in Heterogeneous Catalysis. *J. Mol. Catal. A: Chem.* **1997**, *119*, 405–414.
- (71) Valdés-Pérez, R. E. Algorithm to Generate Reaction Pathways for Computer-Assisted Elucidation. *J. Comput. Chem.* **1992**, *13*, 1079–1088.
- (72) Valdés-Pérez, R. E. Heuristics for Systematic Elucidation of Reaction Pathways. *J. Chem. Inf. Model.* **1994**, *34*, 976–983.
- (73) Rangarajan, S.; Bhan, A.; Daoutidis, P. Language-Oriented Rule-Based Reaction Network Generation and Analysis: Description of RING. *Comput. Chem. Eng.* **2012**, *45*, 114–123.
- (74) Rangarajan, S.; Bhan, A.; Daoutidis, P. Rule-Based Generation of Thermochemical Routes to Biomass Conversion. *Ind. Eng. Chem. Res.* **2010**, *49*, 10459–10470.

- (75) Gao, C. W.; Allen, J. W.; Green, W. H.; West, R. H. Reaction Mechanism Generator: Automatic Construction of Chemical Kinetic Mechanisms. *Comput. Phys. Commun.* **2016**, *203*, 212–225.
- (76) Magoon, G. R.; Green, W. H. Design and Implementation of a Next-Generation Software Interface for on-the-Fly Quantum and Force Field Calculations in Automated Reaction Mechanism Generation. *Comput. Chem. Eng.* **2013**, *52*, 35–45.
- (77) Vernuccio, S.; Broadbelt, L. J. Discerning Complex Reaction Networks Using Automated Generators. *AIChE J.* **2019**, *65*, No. e16663.
- (78) Jalan, A.; West, R. H.; Green, W. H. An Extensible Framework for Capturing Solvent Effects in Computer Generated Kinetic Models. *J. Phys. Chem. B* **2013**, *117*, 2955–2970.
- (79) Varghese, J. J.; Mushrif, S. H. Origins of Complex Solvent Effects on Chemical Reactivity and Computational Tools to Investigate Them: A Review. *React. Chem. Eng.* **2019**, *4*, 165–206.
- (80) Skyner, R. E.; McDonagh, J. L.; Groom, C. R.; Van Mourik, T.; Mitchell, J. B. O. A Review of Methods for the Calculation of Solution Free Energies and the Modelling of Systems in Solution. *Phys. Chem. Chem. Phys.* **2015**, *17*, 6174–6191.
- (81) Saleheen, M.; Heyden, A. Liquid-Phase Modeling in Heterogeneous Catalysis. *ACS Catal.* **2018**, *8*, 2188–2194.
- (82) Dahl, S.; Sehested, J.; Jacobsen, C. J. H.; Törnqvist, E.; Chorkendorff, I. Surface Science Based Microkinetic Analysis of Ammonia Synthesis over Ruthenium Catalysts. *J. Catal.* **2000**, *192*, 391–399.
- (83) Sexton, B. A.; Madix, R. J. A Vibrational Study of Formic Acid Interaction with Clean and Oxygen-Covered Silver (110) Surfaces. *Surf. Sci.* **1981**, *105*, 177–195.
- (84) Wachs, I. E.; Madix, R. J. The Oxidation of Methanol on a Silver (110) Catalyst. *Surf. Sci.* **1978**, *76*, 531–558.
- (85) Schüle, A.; Shekhah, O.; Ranke, W.; Schlögl, R.; Kolios, G. Microkinetic Modelling of the Dehydrogenation of Ethylbenzene to Styrene over Unpromoted Iron Oxides. *J. Catal.* **2005**, *231*, 172–180.
- (86) Andreasen, A.; Lynggaard, H.; Stegelmann, C.; Stoltze, P. A Microkinetic Model of the Methanol Oxidation over Silver. *Surf. Sci.* **2003**, *544*, 5–23.
- (87) Taylor, P. A.; Rasmussen, P. B.; Ovesen, C. V.; Stoltze, P.; Chorkendorff, I. Formate Synthesis on Cu(100). *Surf. Sci.* **1992**, *261*, 191–206.
- (88) Ovesen, C. V.; Stoltze, P.; Nørskov, J. K.; Campbell, C. T. A Kinetic Model of the Water Gas Shift Reaction. *J. Catal.* **1992**, *134*, 445–468.
- (89) Bligaard, T.; Nørskov, J. K. *Chemical Bonding at Surfaces and Interfaces*; Elsevier: Amsterdam, The Netherlands, 2008; Vol. 1.
- (90) Nørskov, J. K.; Abild-Pedersen, F.; Studt, F.; Bligaard, T. Density Functional Theory in Surface Chemistry and Catalysis. *Proc. Natl. Acad. Sci. U. S. A.* **2011**, *108*, 937–943.
- (91) Miura, K.; Watanabe, R.; Fukuhara, C. Theoretical Study of Oxygen Adsorption Energy on Supported Metal Cluster Using D-Band Center Theory and HSAB Concept. *Surf. Sci.* **2020**, *696*, 121601.
- (92) Perdew, J. P.; Burke, K.; Ernzerhof, M. Generalized Gradient Approximation Made Simple. *Phys. Rev. Lett.* **1996**, *77*, 3865–3868.
- (93) Hammer, B.; Nørskov, J. K. Theory of Adsorption and Surface Reactions. In *Chemisorption and Reactivity on Supported Clusters and Thin Films*; Lambert, R. M., Pacchioni, G., Eds.; Springer Netherlands: Amsterdam, 1997; pp 285–351.
- (94) Hammer, B.; Nørskov, J. K. Theoretical Surface Science and Catalysis—Calculations and Concepts. *Adv. Catal.* **2000**, *45*, 71–129.
- (95) Hammer, B.; Hansen, L. B.; Nørskov, J. K. Improved Adsorption Energetics within Density-Functional Theory Using Revised Perdew-Burke-Ernzerhof Functionals. *Phys. Rev. B: Condens. Matter Mater. Phys.* **1999**, *59*, 7413–7421.
- (96) Greeley, J.; Mavrikakis, M. A First-Principles Study of Methanol Decomposition on Pt(111). *J. Am. Chem. Soc.* **2002**, *124*, 7193–7201.
- (97) Mavrikakis, M.; Rempel, J.; Greeley, J.; Hansen, L. B.; Nørskov, J. K. Atomic and Molecular Adsorption on Rh(111). *J. Chem. Phys.* **2002**, *117*, 6737–6744.
- (98) Hammer, B.; Nørskov, J. K. Electronic Factors Determining the Reactivity of Metal Surfaces. *Surf. Sci.* **1995**, *343*, 211–220.
- (99) Hammer, B.; Morikawa, Y.; Nørskov, J. K. CO Chemisorption at Metal Surfaces and Overlayers. *Phys. Rev. Lett.* **1996**, *76*, 2141–2144.
- (100) Fishtik, I.; Datta, R. A UBI-QEP Microkinetic Model for the Water-Gas Shift Reaction on Cu(1 1 1). *Surf. Sci.* **2002**, *512*, 229–254.
- (101) Shustorovich, E.; Zeigarnik, A. V. The UBI-QEP Treatment of Polyatomic Molecules without Bond-Energy Partitioning. *Surf. Sci.* **2003**, *527*, 137–148.
- (102) Sellers, H. The Generalized UBI-QEP Method for Modeling the Energetics of Reactions on Transition Metal Surfaces. *Surf. Sci.* **2003**, *524*, 29–39.
- (103) Gao, X.; Heyden, A.; Abdelrahman, O. A.; Bond, J. Q. Microkinetic Analysis of Acetone Hydrogenation over Pt/SiO<sub>2</sub>. *J. Catal.* **2019**, *374*, 183–198.
- (104) Shiva, M.; Atashi, H.; Tabrizi, F. F.; Mirzaei, A. A. Kinetic Modeling of Fischer-Tropsch Synthesis on Bimetallic Fe-Co Catalyst with Phenomenological Based Approaches. *J. Ind. Eng. Chem.* **2012**, *18*, 1112–1121.
- (105) Mhadeshwar, A. B.; Vlachos, D. G. A Thermodynamically Consistent Surface Reaction Mechanism for CO Oxidation on Pt. *Combust. Flame* **2005**, *142*, 289–298.
- (106) Shustorovich, E.; Bell, A. T. An Analysis of Fischer-Tropsch Synthesis by the Bond-Order-Conservation-Morse-Potential Approach. *Surf. Sci.* **1991**, *248*, 359–368.
- (107) Shustorovich, E. M.; Zeigarnik, A. V. The UBI-QEP Method: Basic Formalism and Applications to Chemisorption Phenomena on Transition Metal Surfaces. *Chemisorption Energetics. Russ. J. Phys. Chem. A* **2006**, *80*, 4–30.
- (108) Greeley, J. Theoretical Heterogeneous Catalysis: Scaling Relationships and Computational Catalyst Design. *Annu. Rev. Chem. Biomol. Eng.* **2016**, *7*, 605–635.
- (109) Liu, B.; Greeley, J. Decomposition Pathways of Glycerol via C-H, O-H, and C-C Bond Scission on Pt(111): A Density Functional Theory Study. *J. Phys. Chem. C* **2011**, *115*, 19702–19709.
- (110) Abild-Pedersen, F.; Greeley, J.; Studt, F.; Rossmeisl, J.; Munter, T. R.; Moses, P. G.; Skúlason, E.; Bligaard, T.; Nørskov, J. K. Scaling Properties of Adsorption Energies for Hydrogen-Containing Molecules on Transition-Metal Surfaces. *Phys. Rev. Lett.* **2007**, *99*, 016105.
- (111) Salciccioli, M.; Chen, Y.; Vlachos, D. G. Density Functional Theory-Derived Group Additivity and Linear Scaling Methods for Prediction of Oxygenate Stability on Metal Catalysts: Adsorption of Open-Ring Alcohol and Polyol Dehydrogenation Intermediates on Pt-Based Metals. *J. Phys. Chem. C* **2010**, *114*, 20155–20166.
- (112) Jones, G.; Jakobsen, J. G.; Shim, S. S.; Kleis, J.; Andersson, M. P.; Rossmeisl, J.; Abild-Pedersen, F.; Bligaard, T.; Helveg, S.; Hinnemann, B.; et al. First Principles Calculations and Experimental Insight into Methane Steam Reforming over Transition Metal Catalysts. *J. Catal.* **2008**, *259*, 147–160.
- (113) Fernández, E. M.; Moses, P. G.; Toftlund, A.; Hansen, H. A.; Martínez, J. I.; Abild-Pedersen, F.; Kleis, J.; Hinnemann, B.; Rossmeisl, J.; Bligaard, T.; et al. Scaling Relationships for Adsorption Energies on Transition Metal Oxide, Sulfide, and Nitride Surfaces. *Angew. Chem., Int. Ed.* **2008**, *47*, 4683–4686.
- (114) Jones, G.; Studt, F.; Abild-Pedersen, F.; Nørskov, J. K.; Bligaard, T. Scaling Relationships for Adsorption Energies of C<sub>2</sub> Hydrocarbons on Transition Metal Surfaces. *Chem. Eng. Sci.* **2011**, *66*, 6318–6323.
- (115) Montemore, M. M.; Medlin, J. W. Scaling Relations between Adsorption Energies for Computational Screening and Design of Catalysts. *Catal. Sci. Technol.* **2014**, *4*, 3748–3761.
- (116) Wijaya, C. D.; Sumathi, R.; Green, W. H. Thermodynamic Properties and Kinetic Parameters for Cyclic Ether Formation from Hydroperoxyalkyl Radicals. *J. Phys. Chem. A* **2003**, *107*, 4908–4920.
- (117) Nicolaides, A.; Rauk, A.; Glukhovtsev, M. N.; Radom, L. Heats of Formation from G<sub>2</sub>, G<sub>2</sub>(MP<sub>2</sub>), and G<sub>2</sub>(MP<sub>2</sub>SVP) Total Energies. *J. Phys. Chem.* **1996**, *100*, 17460–17464.
- (118) Lund, C. R. F. Microkinetics of Water-Gas Shift over Sulfided Mo/Al<sub>2</sub>O<sub>3</sub> Catalysts. *Ind. Eng. Chem. Res.* **1996**, *35*, 2531–2538.

- (119) Aparicio, L. M.; Treviño, A. A.; Rossini, S. A.; Sanfilippo, D. G.; Rekoske, J. E.; Dumesic, J. A. Microkinetic Analysis of Methane Dimerization Reaction. *Ind. Eng. Chem. Res.* **1991**, *30*, 2114–2123.
- (120) Mhadeshwar, A. B.; Wang, H.; Vlachos, D. G. Thermodynamic Consistency in Microkinetic Development of Surface Reaction Mechanisms. *J. Phys. Chem. B* **2003**, *107*, 12721–12733.
- (121) Hill, C. G.; Root, T. W. Basic Concepts in Chemical Kinetics: Molecular Interpretations of Kinetic Phenomena. In *An Introduction to Chemical Engineering Kinetics & Reactor Design*; John Wiley & Sons, Inc.: Hoboken, NJ, 2014; pp 72–116.
- (122) King, D. A. The Influence of Weakly Bound Intermediate States on Thermal Desorption Kinetics. *Surf. Sci.* **1977**, *64*, 43–51.
- (123) Gorte, R.; Schmidt, L. D. Desorption Kinetics with Precursor Intermediates. *Surf. Sci.* **1978**, *76*, 559–573.
- (124) Kisliuk, P. The Sticking Probabilities of Gases Chemisorbed on the Surfaces of Solids-II. *J. Phys. Chem. Solids* **1958**, *5*, 78–84.
- (125) Kisliuk, P. The Sticking Probabilities of Gases Chemisorbed on the Surfaces of Solids. *J. Phys. Chem. Solids* **1957**, *3*, 95–101.
- (126) Rudzinski, W.; Panczyk, T. The Langmuirian Adsorption Kinetics Revised: A Farewell to the XXth Century Theories? *Adsorption* **2002**, *8*, 23–34.
- (127) Boudart, M. *Kinetics of Heterogeneous Catalytic Reactions*, 1st ed.; Butterworth-Heinemann: Stoneham, MA, 1991.
- (128) Henkelman, G.; Jóhannesson, G.; Jónsson, H. Methods for Finding Saddle Points and Minimum Energy Paths. In *Theoretical Methods in Condensed Phase Chemistry - Progress in Theoretical Chemistry and Physics*; Schwartz, S. D., Ed.; Springer Netherlands: New York, 2000; Vol. 5, pp 269–302.
- (129) Henkelman, G.; Jónsson, H. Improved Tangent Estimate in the Nudged Elastic Band Method for Finding Minimum Energy Paths and Saddle Points. *J. Chem. Phys.* **2000**, *113*, 9978–9985.
- (130) Henkelman, G.; Jónsson, H. A Dimer Method for Finding Saddle Points on High Dimensional Potential Surfaces Using Only First Derivatives. *J. Chem. Phys.* **1999**, *111*, 7010–7022.
- (131) Fischer, S.; Karplus, M. Conjugate Peak Refinement: An Algorithm for Finding Reaction Paths and Accurate Transition States in Systems with Many Degrees of Freedom. *Chem. Phys. Lett.* **1992**, *194*, 252–261.
- (132) Mills, G.; Jónsson, H. Quantum and Thermal Effects in H<sub>2</sub> Dissociative Adsorption: Evaluation of Free Energy Barriers in Multidimensional Quantum Systems. *Phys. Rev. Lett.* **1994**, *72*, 1124–1127.
- (133) Fonseca Guerra, C.; Snijders, J. G.; Te Velde, G.; Baerends, E. J. Towards an Order-N DFT Method. *Theor. Chem. Acc.* **1998**, *99*, 391–403.
- (134) Pérez-Jorda, J. M.; Yang, W. An Algorithm for 3D Numerical Integration That Scales Linearly with the Size of the Molecule. *Chem. Phys. Lett.* **1995**, *241*, 469–476.
- (135) Bootsma, A. N.; Wheeler, S. Popular Integration Grids Can Result in Large Errors in DFT-Computed Free Energies. *ChemRxiv* **2019**. DOI: [10.26434/CHEMRXIV.8864204.V4](https://doi.org/10.26434/CHEMRXIV.8864204.V4).
- (136) Shustorovich, E.; Sellers, H. The UBI-QEP Method: A Practical Theoretical Approach to Understanding Chemistry on Transition Metal Surfaces. *Surf. Sci. Rep.* **1998**, *31*, 1–119.
- (137) Callaghan, C.; Fishtik, I.; Datta, R.; Carpenter, M.; Chmielewski, M.; Lugo, A. An Improved Microkinetic Model for the Water Gas Shift Reaction on Copper. *Surf. Sci.* **2003**, *541*, 21–30.
- (138) Jiang, L.; Wang, G. C.; Cai, Z. S.; Pan, Y. M.; Zhao, X. Z. Promotion of the Water-Gas Shift Reaction by Pre-Adsorbed Oxygen on Cu(Hkl) Surfaces: A Theoretical Study. *J. Mol. Struct.: THEOCHEM* **2004**, *710*, 97–104.
- (139) Wang, G.; Jiang, L.; Cai, Z.; Pan, Y.; Zhao, X.; Huang, W.; Xie, K.; Li, Y.; Sun, Y.; Zhong, B. Surface Structure Sensitivity of the Water-Gas Shift Reaction on Cu(Hkl) Surfaces: A Theoretical Study. *J. Phys. Chem. B* **2003**, *107*, 557–562.
- (140) Park, J.; Cho, J.; Lee, Y.; Park, M. J.; Lee, W. B. Practical Microkinetic Modeling Approach for Methanol Synthesis from Syngas over a Cu-Based Catalyst. *Ind. Eng. Chem. Res.* **2019**, *58*, 8663–8673.
- (141) Zeigarnik, A. V.; Shustorovich, E. The UBI-QEP Method: Mechanistic and Kinetic Studies of Heterogeneous Catalytic Reactions. *Russ. J. Phys. Chem. B* **2007**, *1*, 330–356.
- (142) Wang, G.; Zhao, Y.; Cai, Z.; Pan, Y.; Zhao, X.; Li, Y.; Sun, Y.; Zhong, B. Investigation of the Active Sites of CO<sub>2</sub> Hydrogenation to Methanol over a Cu-Based Catalyst by the UBI-QEP Approach. *Surf. Sci.* **2000**, *465*, 51–58.
- (143) Fishtik, I.; Alexander, A.; Datta, R. Enumeration and Discrimination of Mechanisms in Heterogeneous Catalysis Based on Response Reactions and Unity Bond Index-Quadratic Exponential Potential (UBI-QEP) Method. *Surf. Sci.* **1999**, *430*, 1–17.
- (144) Christensen, R.; Hansen, H. A.; Vegge, T. Identifying Systematic DFT Errors in Catalytic Reactions. *Catal. Sci. Technol.* **2015**, *5*, 4946–4949.
- (145) Kim, M. C.; Sim, E.; Burke, K. Understanding and Reducing Errors in Density Functional Calculations. *Phys. Rev. Lett.* **2013**, *111*, 073003.
- (146) Huang, M. H.; Rej, S.; Hsu, S. C. Facet-Dependent Properties of Polyhedral Nanocrystals. *Chem. Commun.* **2014**, *50*, 1634–1644.
- (147) Pal, J.; Pal, T. Faceted Metal and Metal Oxide Nanoparticles: Design, Fabrication and Catalysis. *Nanoscale* **2015**, *7*, 14159–14190.
- (148) Rimer, J. D.; Chawla, A.; Le, T. T. Crystal Engineering for Catalysis. *Annu. Rev. Chem. Biomol. Eng.* **2018**, *9*, 283–309.
- (149) Zhu, B.; Meng, J.; Yuan, W.; Zhang, X.; Yang, H.; Wang, Y.; Gao, Y. Reshaping of Metal Nanoparticles Under Reaction Conditions. *Angew. Chem., Int. Ed.* **2020**, *59*, 2171–2180.
- (150) Tao, F.; Grass, M. E.; Zhang, Y.; Butcher, D. R.; Renzas, J. R.; Liu, Z.; Chung, J. Y.; Mun, B. S.; Salmeron, M.; Somorjai, G. A. Reaction-Driven Restructuring of Rh-Pd and Pt-Pd Core-Shell Nanoparticles. *Science (Washington, DC, U. S.)* **2008**, *322*, 932–934.
- (151) Piccolo, L. Restructuring Effects of the Chemical Environment in Metal Nanocatalysis and Single-Atom Catalysis. *Catal. Today* **2020**, in press.
- (152) Tao, F.; Dag, S.; Wang, L. W.; Liu, Z.; Butcher, D. R.; Bluhm, H.; Salmeron, M.; Somorjai, G. A. Break-up of Stepped Platinum Catalyst Surfaces by High CO Coverage. *Science (Washington, DC, U. S.)* **2010**, *327*, 850–853.
- (153) Sabbe, M. K.; Candela-Rodriguez, G.; Joly, J. F.; Reyniers, M. F.; Marin, G. B. Ab Initio Coverage-Dependent Microkinetic Modeling of Benzene Hydrogenation on Pd(111). *Catal. Sci. Technol.* **2017**, *7*, 5267–5283.
- (154) Lytken, O.; Lew, W.; Campbell, C. T. Catalytic Reaction Energetics by Single Crystal Adsorption Calorimetry: Hydrocarbons on Pt(111). *Chem. Soc. Rev.* **2008**, *37*, 2172–2179.
- (155) Ihm, H.; Ajo, H. M.; Gottfried, J. M.; Bera, P.; Campbell, C. T. Calorimetric Measurement of the Heat of Adsorption of Benzene on Pt(111). *J. Phys. Chem. B* **2004**, *108*, 14627–14633.
- (156) Gokhale, A. A.; Kandoli, S.; Greeley, J. P.; Mavrikakis, M.; Dumesic, J. A. Molecular-Level Descriptions of Surface Chemistry in Kinetic Models Using Density Functional Theory. *Chem. Eng. Sci.* **2004**, *59*, 4679–4691.
- (157) Herron, J. A.; Scaranto, J.; Ferrin, P.; Li, S.; Mavrikakis, M. Trends in Formic Acid Decomposition on Model Transition Metal Surfaces: A Density Functional Theory Study. *ACS Catal.* **2014**, *4*, 4434–4445.
- (158) Jones, G. S.; Mavrikakis, M.; Bartea, M. A.; Vohs, J. M. First Synthesis, Experimental and Theoretical Vibrational Spectra of an Oxametallacycle on a Metal Surface. *J. Am. Chem. Soc.* **1998**, *120*, 3196–3204.
- (159) Medlin, J. W.; Sherrill, A. B.; Chen, J. G.; Bartea, M. A. Experimental and Theoretical Probes of the Structure of Oxametallacycle Intermediates Derived from 1-Epoxy-3-Butene on Ag(110). *J. Phys. Chem. B* **2001**, *105*, 3769–3775.
- (160) Morikawa, Y.; Iwata, K.; Nakamura, J.; Fujitani, T.; Terakura, K. Ab Initio Study of Surface Structural Changes during Methanol Synthesis over Zn/Cu(111). *Chem. Phys. Lett.* **1999**, *304*, 91–97.
- (161) Choksi, T.; Greeley, J. Partial Oxidation of Methanol on MoO<sub>3</sub>(010): A DFT and Microkinetic Study. *ACS Catal.* **2016**, *6*, 7260–7277.

- (162) Zhao, Z. J.; Li, Z.; Cui, Y.; Zhu, H.; Schneider, W. F.; Delgass, W. N.; Ribeiro, F.; Greeley, J. Importance of Metal-Oxide Interfaces in Heterogeneous Catalysis: A Combined DFT, Microkinetic, and Experimental Study of Water-Gas Shift on Au/MgO. *J. Catal.* **2017**, *345*, 157–169.
- (163) Mhadeshwar, A. B.; Vlachos, D. G. Hierarchical, Multiscale Surface Reaction Mechanism Development: CO and H<sub>2</sub> Oxidation, Water-Gas Shift, and Preferential Oxidation of CO on Rh. *J. Catal.* **2005**, *234*, 48–63.
- (164) Deshmukh, S. R.; Mhadeshwar, A. B.; Lebedeva, M. I.; Vlachos, D. G. From Density Functional Theory to Microchemical Device Homogenization: Model Prediction of Hydrogen Production For Portable Fuel Cells. *Int. J. Multiscale Comput. Eng.* **2004**, *2*, 221–238.
- (165) Rubert-Nason, P.; Mavrikakis, M.; Maravelias, C. T.; Grabow, L. C.; Biegler, L. T. Advanced Solution Methods for Microkinetic Models of Catalytic Reactions: A Methanol Synthesis Case Study. *AIChE J.* **2014**, *60*, 1336–1346.
- (166) Demir, B.; Kropp, T.; Rivera-Dones, K. R.; Gilcher, E. B.; Huber, G. W.; Mavrikakis, M.; Dumesic, J. A. A Self-Adjusting Platinum Surface for Acetone Hydrogenation. *Proc. Natl. Acad. Sci. U. S. A.* **2020**, *117*, 3446–3450.
- (167) Weiss, B. M.; Iglesia, E. NO Oxidation Catalysis on Pt Clusters: Elementary Steps, Structural Requirements, and Synergistic Effects of NO<sub>2</sub> Adsorption Sites. *J. Phys. Chem. C* **2009**, *113*, 13331–13340.
- (168) Smeltz, A. D.; Getman, R. B.; Schneider, W. F.; Ribeiro, F. H. Coupled Theoretical and Experimental Analysis of Surface Coverage Effects in Pt-Catalyzed NO and O<sub>2</sub> Reaction to NO<sub>2</sub> on Pt(1 1 1). *Catal. Today* **2008**, *136*, 84–92.
- (169) Getman, R. B.; Schneider, W. F. DFT-Based Coverage-Dependent Model of Pt-Catalyzed NO Oxidation. *ChemCatChem* **2010**, *2*, 1450–1460.
- (170) Motagamwala, A. H.; Ball, M. R.; Dumesic, J. A. Microkinetic Analysis and Scaling Relations for Catalyst Design. *Annu. Rev. Chem. Biomol. Eng.* **2018**, *9*, 413–450.
- (171) Lausche, A. C.; Medford, A. J.; Khan, T. S.; Xu, Y.; Bligaard, T.; Abild-Pedersen, F.; Nørskov, J. K.; Studt, F. On the Effect of Coverage-Dependent Adsorbate-Adsorbate Interactions for CO Methanation on Transition Metal Surfaces. *J. Catal.* **2013**, *307*, 275–282.
- (172) Grabow, L. C.; Hvolbæk, B.; Nørskov, J. K. Understanding Trends in Catalytic Activity: The Effect of Adsorbate-Adsorbate Interactions for CO Oxidation over Transition Metals. *Top. Catal.* **2010**, *53*, 298–310.
- (173) Hellman, A.; Honkala, K. Including Lateral Interactions into Microkinetic Models of Catalytic Reactions. *J. Chem. Phys.* **2007**, *127*, 194704.
- (174) Grabow, L. C.; Gokhale, A. A.; Evans, S. T.; Dumesic, J. A.; Mavrikakis, M. Mechanism of the Water Gas Shift Reaction on Pt: First Principles, Experiments, and Microkinetic Modeling. *J. Phys. Chem. C* **2008**, *112*, 4608–4617.
- (175) Bhandari, S.; Rangarajan, S.; Maravelias, C. T.; Dumesic, J. A.; Mavrikakis, M. Reaction Mechanism of Vapor-Phase Formic Acid Decomposition over Platinum Catalysts: DFT, Reaction Kinetics Experiments, and Microkinetic Modeling. *ACS Catal.* **2020**, *10*, 4112–4126.
- (176) Sluiter, M. H. F.; Kawazoe, Y. Cluster Expansion Method for Adsorption: Application to Hydrogen Chemisorption on Graphene. *Phys. Rev. B: Condens. Matter Mater. Phys.* **2003**, *68*, 085410.
- (177) Tang, H.; Van Der Ven, A.; Trout, B. L. Lateral Interactions between Oxygen Atoms Adsorbed on Platinum (111) by First Principles. *Mol. Phys.* **2004**, *102*, 273–279.
- (178) Schmidt, D. J.; Chen, W.; Wolverton, C.; Schneider, W. F. Performance of Cluster Expansions of Coverage-Dependent Adsorption of Atomic Oxygen on Pt(111). *J. Chem. Theory Comput.* **2012**, *8*, 264–273.
- (179) Stamatakis, M.; Vlachos, D. G. A Graph-Theoretical Kinetic Monte Carlo Framework for on-Lattice Chemical Kinetics. *J. Chem. Phys.* **2011**, *134*, 214115.
- (180) Liu, D.-J.; Evans, J. W. Realistic Multisite Lattice-Gas Modeling and KMC Simulation of Catalytic Surface Reactions: Kinetics and Multiscale Spatial Behavior for CO-Oxidation on Metal (100) Surfaces. *Prog. Surf. Sci.* **2013**, *88*, 393–521.
- (181) Matera, S.; Schneider, W. F.; Heyden, A.; Savara, A. Progress in Accurate Chemical Kinetic Modeling, Simulations, and Parameter Estimation for Heterogeneous Catalysis. *ACS Catal.* **2019**, *9*, 6624–6647.
- (182) Dumesic, J. A. Reply to Finding the Rate-Determining Step in a Mechanism: Comparing DeDonder Relations with the “Degree of Rate Control”. *J. Catal.* **2001**, *204*, 525–529.
- (183) Campbell, C. T. Finding the Rate-Determining Step in a Mechanism: Comparing DeDonder Relations with the “Degree of Rate Control”. *J. Catal.* **2001**, *204*, 520–524.
- (184) Dumesic, J. A. Analyses of Reaction Schemes Using De Donder Relations. *J. Catal.* **1999**, *185*, 496–505.
- (185) Cortright, R. D.; Dumesic, J. A. Kinetics of Heterogeneous Catalytic Reactions: Analysis of Reaction Schemes. *Adv. Catal.* **2001**, *46*, 161–264.
- (186) Linic, S.; Bartea, M. A. Construction of a Reaction Coordinate and a Microkinetic Model for Ethylene Epoxidation on Silver from DFT Calculations and Surface Science Experiments. *J. Catal.* **2003**, *214*, 200–212.
- (187) Cortright, R. D.; Watwe, R. M.; Dumesic, J. A. Ethane Hydrogenolysis over Platinum Selection and Estimation of Kinetic Parameters. *J. Mol. Catal. A: Chem.* **2000**, *163*, 91–103.
- (188) Gounder, R.; Iglesia, E. Catalytic Hydrogenation of Alkenes on Acidic Zeolites: Mechanistic Connections to Monomolecular Alkane Dehydrogenation Reactions. *J. Catal.* **2011**, *277*, 36–45.
- (189) Campbell, C. T. Future Directions and Industrial Perspectives Micro- and Macro-Kinetics: Their Relationship in Heterogeneous Catalysis. *Top. Catal.* **1994**, *1*, 353–366.
- (190) Stegelmann, C.; Andreasen, A.; Campbell, C. T. Degree of Rate Control: How Much the Energies of Intermediates and Transition States Control Rates. *J. Am. Chem. Soc.* **2009**, *131*, 8077–8082.
- (191) Sanchez-Castillo, M. A.; Agarwal, N.; Miller, C.; Cortright, R. D.; Madon, R. J.; Dumesic, J. A. Reaction Kinetics Study and Analysis of Reaction Schemes for Isobutane Conversion over USY Zeolite. *J. Catal.* **2002**, *205*, 67–85.
- (192) Grabow, L.; Xu, Y.; Mavrikakis, M. Lattice Strain Effects on CO Oxidation on Pt(111). *Phys. Chem. Chem. Phys.* **2006**, *8*, 3369–3374.
- (193) Stegelmann, C.; Schiødt, N. C.; Campbell, C. T.; Stoltze, P. Microkinetic Modeling of Ethylene Oxidation over Silver. *J. Catal.* **2004**, *221*, 630–649.
- (194) Campbell, C. T. The Degree of Rate Control: A Powerful Tool for Catalysis Research. *ACS Catal.* **2017**, *7*, 2770–2779.
- (195) Studt, F.; Behrens, M.; Kunkes, E. L.; Thomas, N.; Zander, S.; Tarasov, A.; Schumann, J.; Frei, E.; Varley, J. B.; Abild-Pedersen, F.; et al. The Mechanism of CO and CO<sub>2</sub> Hydrogenation to Methanol over Cu-Based Catalysts. *ChemCatChem* **2015**, *7*, 1105–1111.
- (196) Mao, Z.; Campbell, C. T. Apparent Activation Energies in Complex Reaction Mechanisms: A Simple Relationship via Degrees of Rate Control. *ACS Catal.* **2019**, *9*, 9465–9473.
- (197) Mao, Z.; Campbell, C. T. Kinetic Isotope Effects: Interpretation and Prediction Using Degrees of Rate Control. *ACS Catal.* **2020**, *10*, 4181–4192.
- (198) Medford, A. J.; Vojvodic, A.; Hummelshøj, J. S.; Voss, J.; Abild-Pedersen, F.; Studt, F.; Bligaard, T.; Nilsson, A.; Nørskov, J. K. From the Sabatier Principle to a Predictive Theory of Transition-Metal Heterogeneous Catalysis. *J. Catal.* **2015**, *328*, 36–42.
- (199) Aika, K.; Ozaki, A. Catalysts for Synthesis of Ammonia. In *Catalysis, Science and Technology*; Anderson, J. R., Boudart, M., Eds.; Springer Verlag: Berlin, 1981; p 88.
- (200) Mavrikakis, M.; Hammer, B.; Nørskov, J. K. Effect of Strain on the Reactivity of Metal Surfaces. *Phys. Rev. Lett.* **1998**, *81*, 2819–2822.
- (201) Kitchin, J. R.; Nørskov, J. K.; Bartea, M. A.; Chen, J. G. Role of Strain and Ligand Effects in the Modification of the Electronic and Chemical Properties of Bimetallic Surfaces. *Phys. Rev. Lett.* **2004**, *93*, 156801.
- (202) Nørskov, J. K.; Stoltze, P. Theoretical Aspects of Surface Reactions. *Surf. Sci.* **1987**, *189–190*, 91–105.

- (203) Nørskov, J. K.; Bligaard, T.; Logadottir, A.; Bahn, S.; Hansen, L. B.; Bollinger, M.; Bengaard, H.; Hammer, B.; Sljivancanin, Z.; Mavrikakis, M.; et al. Universality in Heterogeneous Catalysis. *J. Catal.* **2002**, *209*, 275–278.
- (204) Evans, M. G.; Polanyi, M. Inertia and Driving Force of Chemical Reactions. *Trans. Faraday Soc.* **1938**, *34*, 11–24.
- (205) van Santen, R. A.; Neurock, M.; Shetty, S. G. Reactivity Theory of Transition-Metal Surfaces: A Brønsted-Evans-Polanyi Linear Activation Energy-Free-Energy Analysis. *Chem. Rev.* **2010**, *110*, 2005–2048.
- (206) Vojvodic, A.; Calle-Vallejo, F.; Guo, W.; Wang, S.; Toftlund, A.; Studt, F.; Martínez, J. I.; Shen, J.; Man, I. C.; Rossmeisl, J.; et al. On the Behavior of Brønsted-Evans-Polanyi Relations for Transition Metal Oxides. *J. Chem. Phys.* **2011**, *134*, 244509.
- (207) Ferrin, P.; Simonetti, D.; Kandoi, S.; Kunkes, E.; Dumesic, J. A.; Nørskov, J. K.; Mavrikakis, M. Modeling Ethanol Decomposition on Transition Metals: A Combined Application of Scaling and Brønsted-Evans-Polanyi Relations. *J. Am. Chem. Soc.* **2009**, *131*, 5809–5815.
- (208) Loffreda, D.; Delbecq, F.; Vigné, F.; Sautet, P. Fast Prediction of Selectivity in Heterogeneous Catalysis from Extended Brønsted-Evans-Polanyi Relations: A Theoretical Insight. *Angew. Chem., Int. Ed.* **2009**, *48*, 8978–8980.
- (209) Jacobsen, C. J. H.; Dahl, S.; Clausen, B. G. S.; Bahn, S.; Logadottir, A.; Nørskov, J. K. Catalyst Design by Interpolation in the Periodic Table: Bimetallic Ammonia Synthesis Catalysts. *J. Am. Chem. Soc.* **2001**, *123*, 8404–8405.
- (210) Sutton, J. E.; Vlachos, D. G. A Theoretical and Computational Analysis of Linear Free Energy Relations for the Estimation of Activation Energies. *ACS Catal.* **2012**, *2*, 1624–1634.
- (211) Loffreda, D.; Delbecq, F.; Vigné, F.; Sautet, P. Chemo-Regioselectivity in Heterogeneous Catalysis: Competitive Routes for C=O and C=C Hydrogenations from a Theoretical Approach. *J. Am. Chem. Soc.* **2006**, *128*, 1316–1323.
- (212) Zhao, Z. J.; Liu, S.; Zha, S.; Cheng, D.; Studt, F.; Henkelman, G.; Gong, J. Theory-Guided Design of Catalytic Materials Using Scaling Relationships and Reactivity Descriptors. *Nat. Rev. Mater.* **2019**, *4*, 792–804.
- (213) Grabow, L. C.; Studt, F.; Abild-Pedersen, F.; Petzold, V.; Kleis, J.; Bligaard, T.; Nørskov, J. K. Descriptor-Based Analysis Applied to HCN Synthesis from NH<sub>3</sub> and CH<sub>4</sub>. *Angew. Chem., Int. Ed.* **2011**, *50*, 4601–4605.
- (214) Anand, M.; Nørskov, J. K. Scaling Relations in Homogeneous Catalysis: Analyzing the Buchwald-Hartwig Amination Reaction. *ACS Catal.* **2020**, *10*, 336–345.
- (215) Toftlund, A.; Man, I. C.; Hansen, H. A.; Abild-Pedersen, F.; Bligaard, T.; Rossmeisl, J.; Studt, F. Volcano Relations for Oxidation of Hydrogen Halides over Rutile Oxide Surfaces. *ChemCatChem* **2012**, *4*, 1856–1861.
- (216) Jørgensen, M.; Grönbeck, H. Perspectives on Computational Catalysis for Metal Nanoparticles. *ACS Catal.* **2019**, *9*, 8872–8881.
- (217) Assary, R. S.; Broadbelt, L. J.; Curtiss, L. A. Brønsted-Evans-Polanyi Relationships for C-C Bond Forming and C-C Bond Breaking Reactions in Thiamine-Catalyzed Decarboxylation of 2-Keto Acids Using Density Functional Theory. *J. Mol. Model.* **2012**, *18*, 145–150.
- (218) Wang, S.; Vorotnikov, V.; Sutton, J. E.; Vlachos, D. G. Brønsted-Evans-Polanyi and Transition State Scaling Relations of Furan Derivatives on Pd(111) and Their Relation to Those of Small Molecules. *ACS Catal.* **2014**, *4*, 604–612.
- (219) Greeley, J.; Mavrikakis, M. Alloy Catalysts Designed from First Principles. *Nat. Mater.* **2004**, *3*, 810–815.
- (220) Medford, A. J.; Lausche, A. C.; Abild-Pedersen, F.; Temel, B.; Schjødt, N. C.; Nørskov, J. K.; Studt, F. Activity and Selectivity Trends in Synthesis Gas Conversion to Higher Alcohols. *Top. Catal.* **2014**, *57*, 135–142.
- (221) Wang, S.; Temel, B.; Shen, J.; Jones, G.; Grabow, L. C.; Studt, F.; Bligaard, T.; Abild-Pedersen, F.; Christensen, C. H.; Nørskov, J. K. Universal Brønsted-Evans-Polanyi Relations for C-C, C-O, C-N, N-O, N-N, and O-O Dissociation Reactions. *Catal. Lett.* **2011**, *141*, 370–373.
- (222) Wang, Y.; Xiao, L.; Qi, Y.; Mahmoodinia, M.; Feng, X.; Yang, J.; Zhu, Y. A.; Chen, D. Towards Rational Catalyst Design: Boosting the Rapid Prediction of Transition-Metal Activity by Improved Scaling Relations. *Phys. Chem. Chem. Phys.* **2019**, *21*, 19269–19280.
- (223) Choksi, T. S.; Streibel, V.; Abild-Pedersen, F. Predicting Metal-Metal Interactions. II. Accelerating Generalized Schemes through Physical Insights. *J. Chem. Phys.* **2020**, *152*, 152.
- (224) Studt, F.; Abild-Pedersen, F.; Hansen, H.; Man, I.; Rossmeisl, J.; Bligaard, T. Volcano Relation for the Deacon Process over Transition-Metal Oxides. *ChemCatChem* **2010**, *2*, 98–102.
- (225) Bligaard, T.; Nørskov, J. K.; Dahl, S.; Matthiesen, J.; Christensen, C. H.; Sehested, J. The Brønsted-Evans-Polanyi Relation and the Volcano Curve in Heterogeneous Catalysis. *J. Catal.* **2004**, *224*, 206–217.
- (226) Wang, S.; Petzold, V.; Tripkovic, V.; Kleis, J.; Howalt, J. G.; Skúlason, E.; Fernández, E. M.; Hvolbæk, B.; Jones, G.; Toftlund, A.; et al. Universal Transition State Scaling Relations for (de)-Hydrogenation over Transition Metals. *Phys. Chem. Chem. Phys.* **2011**, *13*, 20760–20765.
- (227) Zaffran, J.; Michel, C.; Auneau, F.; Delbecq, F.; Sautet, P. Linear Energy Relations as Predictive Tools for Polyalcohol Catalytic Reactivity. *ACS Catal.* **2014**, *4*, 464–468.
- (228) Lee, K.; Gu, G. H.; Mullen, C. A.; Boateng, A. A.; Vlachos, D. G. Guaiacol Hydrodeoxygenation Mechanism on Pt(111): Insights from Density Functional Theory and Linear Free Energy Relations. *ChemSusChem* **2015**, *8*, 315–322.
- (229) Sutton, J. E.; Guo, W.; Katsoulakis, M. A.; Vlachos, D. G. Effects of Correlated Parameters and Uncertainty in Electronic-Structure-Based Chemical Kinetic Modelling. *Nat. Chem.* **2016**, *8*, 331–337.
- (230) Sutton, J. E.; Vlachos, D. G. Effect of Errors in Linear Scaling Relations and Brønsted-Evans-Polanyi Relations on Activity and Selectivity Maps. *J. Catal.* **2016**, *338*, 273–283.
- (231) Wolcott, C. A.; Medford, A. J.; Studt, F.; Campbell, C. T. Degree of Rate Control Approach to Computational Catalyst Screening. *J. Catal.* **2015**, *330*, 197–207.
- (232) Xu, Z.; Kitchin, J. R. Probing the Coverage Dependence of Site and Adsorbate Configurational Correlations on (111) Surfaces of Late Transition Metals. *J. Phys. Chem. C* **2014**, *118*, 25597–25602.
- (233) Avanesian, T.; Christopher, P. Scaled Degree of Rate Control: Identifying Elementary Steps That Control Differences in Performance of Transition-Metal Catalysts. *ACS Catal.* **2016**, *6*, 5268–5272.
- (234) Baumes, L. A.; Serra, J. M.; Serna, P.; Corma, A. Support Vector Machines for Predictive Modeling in Heterogeneous Catalysis: A Comprehensive Introduction and Overfitting Investigation Based on Two Real Applications. *J. Comb. Chem.* **2006**, *8*, 583–596.
- (235) Hattori, T.; Kito, S. Neural Network as a Tool for Catalyst Development. *Catal. Today* **1995**, *23*, 347–355.
- (236) Jinnouchi, R.; Asahi, R. Predicting Catalytic Activity of Nanoparticles by a DFT-Aided Machine-Learning Algorithm. *J. Phys. Chem. Lett.* **2017**, *8*, 4279–4283.
- (237) Ulissi, Z. W.; Tang, M. T.; Xiao, J.; Liu, X.; Torelli, D. A.; Karamad, M.; Cummins, K.; Hahn, C.; Lewis, N. S.; Jaramillo, T. F.; et al. Machine-Learning Methods Enable Exhaustive Searches for Active Bimetallic Facets and Reveal Active Site Motifs for CO<sub>2</sub> Reduction. *ACS Catal.* **2017**, *7*, 6600–6608.
- (238) Smith, A.; Keane, A.; Dumesic, J. A.; Huber, G. W.; Zavala, V. M. A Machine Learning Framework for the Analysis and Prediction of Catalytic Activity from Experimental Data. *Appl. Catal., B* **2020**, *263*, 118257.
- (239) Noh, J.; Back, S.; Kim, J.; Jung, Y. Active Learning with Non-Ab Initio Input Features toward Efficient CO<sub>2</sub> Reduction Catalysts. *Chem. Sci.* **2018**, *9*, 5152–5159.
- (240) Botu, V.; Batra, R.; Chapman, J.; Ramprasad, R. Machine Learning Force Fields: Construction, Validation, and Outlook. *J. Phys. Chem. C* **2017**, *121*, 511–522.
- (241) Brockherde, F.; Vogt, L.; Li, L.; Tuckerman, M. E.; Burke, K.; Müller, K. R. Bypassing the Kohn-Sham Equations with Machine Learning. *Nat. Commun.* **2017**, *8*, 1–10.

- (242) Behler, J. First Principles Neural Network Potentials for Reactive Simulations of Large Molecular and Condensed Systems. *Angew. Chem., Int. Ed.* **2017**, *56*, 12828–12840.
- (243) Goldsmith, B. R.; Esterhuizen, J.; Liu, J.; Bartel, C. J.; Sutton, C. Machine Learning for Heterogeneous Catalyst Design and Discovery. *AIChE J.* **2018**, *64*, 2311–2323.
- (244) Dahl, S.; Logadottir, A.; Jacobsen, C. J. H.; Nørskov, J. K. Electronic Factors in Catalysis: The Volcano Curve and the Effect of Promotion in Catalytic Ammonia Synthesis. *Appl. Catal., A* **2001**, *222*, 19–29.
- (245) Sperger, T.; Fisher, H. C.; Schoenebeck, F. Computationally Deciphering Palladium-Catalyzed Reaction Mechanisms. *Wiley Interdiscip. Rev. Comput. Mol. Sci.* **2016**, *6*, 226–242.
- (246) Sameera, W. M. C.; Maseras, F. Transition Metal Catalysis by Density Functional Theory and Density Functional Theory/Molecular Mechanics. *Wiley Interdiscip. Rev. Comput. Mol. Sci.* **2012**, *2*, 375–385.
- (247) Santoro, S.; Kalek, M.; Huang, G.; Himo, F. Elucidation of Mechanisms and Selectivities of Metal-Catalyzed Reactions Using Quantum Chemical Methodology. *Acc. Chem. Res.* **2016**, *49*, 1006–1018.
- (248) Carbó, J. J.; Maseras, F.; Bo, C.; van Leeuwen, P. W. N. M. Unraveling the Origin of Regioselectivity in Rhodium Diphosphine Catalyzed Hydroformylation. A DFT QM/MM Study. *J. Am. Chem. Soc.* **2001**, *123*, 7630–7637.
- (249) Ying, F.; Zhang, Y.; Xiang, C.; Song, Z.; Xie, H.; Bao, W. Key Mechanistic Features in Palladium-Catalyzed Methylcyclopropanation of Norbornenes with Vinyl Bromides: Insights from DFT Calculations. *Front. Chem.* **2019**, *7*, 169.
- (250) Zhang, X.; Li, P.; Wang, B.; Cao, Z. Mechanistic Features in Al(I)-Mediated Oxidative Addition of Aryl C-F Bonds: Insights From Density Functional Theory Calculations. *Front. Chem.* **2019**, *7*, 596.
- (251) Sun, Q.; Hong, P.; Wei, D.; Wu, A.; Tan, K.; Lu, X. Chemoselectivity in Gold(I)-Catalyzed Propargyl Ester Reactions: Insights From DFT Calculations. *Front. Chem.* **2019**, *7*, 609.
- (252) Chmely, S. C.; Kim, S.; Ciesielski, P. N.; Jiménez-Osés, G.; Paton, R. S.; Beckham, G. T. Mechanistic Study of a Ru-Xantphos Catalyst for Tandem Alcohol Dehydrogenation and Reductive Aryl-Ether Cleavage. *ACS Catal.* **2013**, *3*, 963–974.
- (253) Braga, A. A. C.; Caballero, A.; Urbano, J.; Diaz-Requejo, M. M.; Pérez, P. J.; Maseras, F. Mechanism of Side Reactions in Alkane C-H Bond Functionalization by Diazo Compounds Catalyzed by Ag and Cu Homoscorpionate Complexes-A DFT Study. *ChemCatChem* **2011**, *3*, 1646–1652.
- (254) Marini, S.; Salvi, P.; Nelli, P.; Pesenti, R.; Villa, M.; Berrettoni, M.; Zangari, G.; Kiros, Y. Advanced Alkaline Water Electrolysis. *Electrochim. Acta* **2012**, *82*, 384–391.
- (255) Suen, N. T.; Hung, S. F.; Quan, Q.; Zhang, N.; Xu, Y. J.; Chen, H. M. Electrocatalysis for the Oxygen Evolution Reaction: Recent Development and Future Perspectives. *Chem. Soc. Rev.* **2017**, *46*, 337–365.
- (256) Li, P.; Zhao, R.; Chen, H.; Wang, H.; Wei, P.; Huang, H.; Liu, Q.; Li, T.; Shi, X.; Zhang, Y.; et al. Recent Advances in the Development of Water Oxidation Electrocatalysts at Mild pH. *Small* **2019**, *15*, 1805103.
- (257) Carrette, L.; Friedrich, K. A.; Stimming, U. Fuel Cells - Fundamentals and Applications. *Fuel Cells* **2001**, *1*, 5–39.
- (258) Jamesh, M. I. Recent Progress on Earth Abundant Hydrogen Evolution Reaction and Oxygen Evolution Reaction Bifunctional Electrocatalyst for Overall Water Splitting in Alkaline Media. *J. Power Sources* **2016**, *333*, 213–236.
- (259) McCrory, C. C. L.; Jung, S.; Peters, J. C.; Jaramillo, T. F. Benchmarking Heterogeneous Electrocatalysts for the Oxygen Evolution Reaction. *J. Am. Chem. Soc.* **2013**, *135*, 16977–16987.
- (260) Strmcnik, D.; Uchimura, M.; Wang, C.; Subbaraman, R.; Danilovic, N.; Van Der Vliet, D.; Paulikas, A. P.; Stamenkovic, V. R.; Markovic, N. M. Improving the Hydrogen Oxidation Reaction Rate by Promotion of Hydroxyl Adsorption. *Nat. Chem.* **2013**, *5*, 300–306.
- (261) Kahyarian, A.; Brown, B.; Nesic, S. Mechanism of the Hydrogen Evolution Reaction in Mildly Acidic Environments on Gold. *J. Electrochem. Soc.* **2017**, *164*, H365–H374.
- (262) Popczun, E. J.; Read, C. G.; Roske, C. W.; Lewis, N. S.; Schaak, R. E. Highly Active Electrocatalysis of the Hydrogen Evolution Reaction by Cobalt Phosphide Nanoparticles. *Angew. Chem., Int. Ed.* **2014**, *53*, 5427–5430.
- (263) Moon, J. S.; Jang, J. H.; Kim, E. G.; Chung, Y. H.; Yoo, S. J.; Lee, Y. K. The Nature of Active Sites of Ni<sub>2</sub>P Electrocatalyst for Hydrogen Evolution Reaction. *J. Catal.* **2015**, *326*, 92–99.
- (264) Hansen, H. A.; Viswanathan, V.; Nørskov, J. K. Unifying Kinetic and Thermodynamic Analysis of 2 e- and 4 e- Reduction of Oxygen on Metal Surfaces. *J. Phys. Chem. C* **2014**, *118*, 6706–6718.
- (265) Holewinski, A.; Linic, S. Elementary Mechanisms in Electrocatalysis: Revisiting the ORR Tafel Slope. *J. Electrochem. Soc.* **2012**, *159*, H864–H870.
- (266) Quaino, P. M.; Gennero de Chialvo, M. R.; Chialvo, A. C. Hydrogen Electrode Reaction: A Complete Kinetic Description. *Electrochim. Acta* **2007**, *52*, 7396–7403.
- (267) Wang, J. X.; Markovic, N. M.; Adzic, R. R. Kinetic Analysis of Oxygen Reduction on Pt(111) in Acid Solutions: Intrinsic Kinetic Parameters and Anion Adsorption Effects. *J. Phys. Chem. B* **2004**, *108*, 4127–4133.
- (268) Tavares, M. C.; Machado, S. A. S.; Mazo, L. H. Study of Hydrogen Evolution Reaction in Acid Medium on Pt Microelectrodes. *Electrochim. Acta* **2001**, *46*, 4359–4369.
- (269) Arce, M. D.; Bonazza, H. L.; Fernández, J. L. Kinetic Analysis of the Hydrogen Electrode Reaction in Unbuffered Media. Theory and Studies on Pt Microelectrodes. *Electrochim. Acta* **2013**, *107*, 248–260.
- (270) Auinger, M.; Katsounaros, I.; Meier, J. C.; Klemm, S. O.; Biedermann, P. U.; Topalov, A. A.; Rohwerder, M.; Mayrhofer, K. J. J. Near-Surface Ion Distribution and Buffer Effects during Electrochemical Reactions. *Phys. Chem. Chem. Phys.* **2011**, *13*, 16384–16394.
- (271) Carneiro-Neto, E. B.; Lopes, M. C.; Pereira, E. C. Simulation of Interfacial pH Changes during Hydrogen Evolution Reaction. *J. Electroanal. Chem.* **2016**, *765*, 92–99.
- (272) Shinagawa, T.; Garcia-Esparza, A. T.; Takanabe, K. Insight on Tafel Slopes from a Microkinetic Analysis of Aqueous Electrocatalysis for Energy Conversion. *Sci. Rep.* **2015**, *5*, 1–21.
- (273) Kuhl, K. P.; Cave, E. R.; Abram, D. N.; Jaramillo, T. F. New Insights into the Electrochemical Reduction of Carbon Dioxide on Metallic Copper Surfaces. *Energy Environ. Sci.* **2012**, *5*, 7050–7059.
- (274) Tang, W.; Peterson, A. A.; Varela, A. S.; Jovanov, Z. P.; Bech, L.; Durand, W. J.; Dahl, S.; Nørskov, J. K.; Chorkendorff, I. The Importance of Surface Morphology in Controlling the Selectivity of Polycrystalline Copper for CO<sub>2</sub> Electroreduction. *Phys. Chem. Chem. Phys.* **2012**, *14*, 76–81.
- (275) Kas, R.; Kortlever, R.; Yilmaz, H.; Koper, M. T. M.; Mul, G. Manipulating the Hydrocarbon Selectivity of Copper Nanoparticles in CO<sub>2</sub> Electroreduction by Process Conditions. *ChemElectroChem* **2015**, *2*, 354–358.
- (276) Schouten, K. J. P.; Kwon, Y.; Van Der Ham, C. J. M.; Qin, Z.; Koper, M. T. M. A New Mechanism for the Selectivity to C<sub>1</sub> and C<sub>2</sub> Species in the Electrochemical Reduction of Carbon Dioxide on Copper Electrodes. *Chem. Sci.* **2011**, *2*, 1902–1909.
- (277) Heyes, J.; Dunwell, M.; Xu, B. CO<sub>2</sub> Reduction on Cu at Low Overpotentials with Surface-Enhanced In Situ Spectroscopy. *J. Phys. Chem. C* **2016**, *120*, 17334–17341.
- (278) Wuttig, A.; Liu, C.; Peng, Q.; Yaguchi, M.; Hendon, C. H.; Motobayashi, K.; Ye, S.; Osawa, M.; Surendranath, Y. Tracking a Common Surface-Bound Intermediate during CO<sub>2</sub>-to- Fuels Catalysis. *ACS Cent. Sci.* **2016**, *2*, 522–528.
- (279) Figueiredo, M. C.; Ledezma-Yanez, I.; Koper, M. T. M. In Situ Spectroscopic Study of CO<sub>2</sub> Electroreduction at Copper Electrodes in Acetonitrile. *ACS Catal.* **2016**, *6*, 2382–2392.
- (280) Wiebe, J.; Kravchenko, K.; Spohr, E. Electrolyte Effects in a Model of Proton Discharge on Charged Electrodes. *Surf. Sci.* **2015**, *631*, 35–41.

- (281) Härtel, A. Structure of Electric Double Layers in Capacitive Systems and to What Extent (Classical) Density Functional Theory Describes It. *J. Phys.: Condens. Matter* **2017**, *29*, 423002.
- (282) Zhu, S.; Jiang, B.; Cai, W.; Bin Shao, M. Direct Observation on Reaction Intermediates and the Role of Bicarbonate Anions in CO<sub>2</sub> Electrochemical Reduction Reaction on Cu Surfaces. *J. Am. Chem. Soc.* **2017**, *139*, 15664–15667.
- (283) Burch, R. The Investigation of Mechanisms in Environmental Catalysis Using Time-Resolved Methods. *Top. Catal.* **2003**, *24*, 97–102.
- (284) Avgouropoulos, G. Isotopic Transient Study of Methanol Decomposition over Noble Metal/Ceria Catalysts. *Catal. Commun.* **2009**, *10*, 682–686.
- (285) Sadovskaya, E. M.; Suknev, A. P.; Goncharov, V. B.; Bal'zhinimaev, B. S.; Mirodatos, C. Reaction Kinetics and Mechanism of Selective NO Reduction on a CoZSM-5 Catalyst as Studied by SSITKA. *Kinet. Catal.* **2004**, *45*, 436–445.
- (286) Nijhuis, T. A.; Sacaliuc-Parvulescu, E.; Govender, N. S.; Schouten, J. C.; Weckhuysen, B. M. The Role of Support Oxygen in the Epoxidation of Propene over Gold-Titania Catalysts Investigated by Isotopic Transient Kinetics. *J. Catal.* **2009**, *265*, 161–169.
- (287) Polychronopoulou, K.; Efsthathiou, A. M. Spillover of Labile OH, H, and O Species in the H<sub>2</sub> Production by Steam Reforming of Phenol over Supported-Rh Catalysts. *Catal. Today* **2006**, *116*, 341–347.
- (288) Sadovskaya, E. M.; Suknev, A. P.; Pinaeva, L. G.; Goncharov, V. B.; Bal'zhinimaev, B. S.; Chupin, C.; Pérez-Ramírez, J.; Mirodatos, C. Mechanism and Kinetics of the Selective NO Reduction over Co-ZSM-5 Studied by the SSITKA Technique: 2. Reactivity of NO<sub>x</sub>-Adsorbed Species with Methane. *J. Catal.* **2004**, *225*, 179–189.
- (289) Granger, P.; Pietrzyk, S. Steady-State and Unsteady-State Kinetic Approaches for Studying Reactions over Three-Way Natural Gas Vehicle Catalysts. *C. R. Chim.* **2014**, *17*, 656–671.
- (290) Patanou, E.; Lillebø, A. H.; Yang, J.; Chen, D.; Holmen, A.; Blekkan, E. A. Microcalorimetric Studies on Co-Re/γ-Al<sub>2</sub>O<sub>3</sub> Catalysts with Na Impurities for Fischer–Tropsch Synthesis. *Ind. Eng. Chem. Res.* **2014**, *53*, 1787–1793.
- (291) Yang, J.; Chen, D.; Holmen, A. Understanding the Kinetics and Re Promotion of Carbon Nanotube Supported Cobalt Catalysts by SSITKA. *Catal. Today* **2012**, *186*, 99–108.
- (292) Zijlstra, B.; Broos, R. J. P.; Chen, W.; Filot, I. A. W.; Hensen, E. J. M. First-Principles Based Microkinetic Modeling of Transient Kinetics of CO Hydrogenation on Cobalt Catalysts. *Catal. Today* **2020**, *342*, 131–141.
- (293) Filot, I. A. W.; van Santen, R. A.; Hensen, E. J. M. The Optimally Performing Fischer–Tropsch Catalyst. *Angew. Chem., Int. Ed.* **2014**, *53*, 12746–12750.
- (294) Filot, I. A. W.; Broos, R. J. P.; Van Rijn, J. P. M.; Van Heugten, G. J. H. A.; Van Santen, R. A.; Hensen, E. J. M. First-Principles-Based Microkinetics Simulations of Synthesis Gas Conversion on a Stepped Rhodium Surface. *ACS Catal.* **2015**, *5*, 5453–5467.
- (295) Omojola, T.; Lukyanov, D. B.; Veen, A. C. Transient Kinetic Studies and Microkinetic Modeling of Primary Olefin Formation from Dimethyl Ether over ZSM-5 Catalysts. *Int. J. Chem. Kinet.* **2019**, *51*, S28–S37.
- (296) Van Dijk, H. A. J.; Hoebink, J. H. B. J.; Schouten, J. C. A Mechanistic Study of the Fischer–Tropsch Synthesis Using Transient Isotopic Tracing. Part-1: Model Identification and Discrimination. *Top. Catal.* **2003**, *26*, 111–119.
- (297) Gerceker, D.; Motagamwala, A. H.; Rivera-Dones, K. R.; Miller, J. B.; Huber, G. W.; Mavrikakis, M.; Dumesic, J. A. Methane Conversion to Ethylene and Aromatics on PtSn Catalysts. *ACS Catal.* **2017**, *7*, 2088–2100.
- (298) Campbell, C. T.; Sellers, J. R. V. The Entropies of Adsorbed Molecules. *J. Am. Chem. Soc.* **2012**, *134*, 18109–18115.